Ground Penetrating Radar Imaging Prehistoric Animal Skeletons and Paleofeatures in Ash Beds at Ashfall Fossil Beds Historical State Park, Nebraska

By

Michelle Proulx
B.S. Geology, James Madison University, 2018

Submitted to the graduate degree program in Department of Geology and the Graduate Faculty of the University of Kansas in partial fulfillment of the requirements for the degree of Master of Science.

George Tsoflias, Co-Chair

Rolfe Mandel, Co-Chair

Chi Zhang

Date Defended: May 26, 2021

The Thesis Committee for Michelle Proulx certifies that this is the approved version of the following thesis:

Ground Penetrating Radar Imaging Prehistoric Animal Skeletons and Paleofeatures in ash beds at Ashfall Fossil Beds Historical State Park, Nebraska

Co-Chair: George Tsoflias

Co-Chair: Rolfe Mandel

Date Approved: September 4, 2021

Abstract

Ground penetrating radar (GPR) is a non-invasive imaging method of the shallow subsurface. However, prior to my study, the capabilities of GPR for imaging bones encased in fine volcanic ash deposits had not been determined. To evaluate those capabilities, I tested 500 MHz and 1 GHz frequency GPR on 11.86 ± 0.13-million-year-old bone assemblages buried in fine *Konservat-Lagerstätte* ash deposits at Ashfall Fossil Beds State Historical Park in northeastern Nebraska. The main objectives of this research are to test the ability of GPR to image ash beds, buried animal skeletons and ichnofossils, and map their presence across the site. For this investigation, I acquired 173 GPR lines in dense grids covering approximately 220 m^2 of the unexcavated section of the Hubbard Barn at Ashfall.

Fine volcanic ash is a low electrical conductivity environment that favors GPR imaging due to low attenuation of radar signals. GPR images ash layers as strong continuous reflections. Both the 500 MHz and 1 GHz GPR frequencies imaged through the entire thickness of ash deposits, detecting the interface with the underlying sandstone at depths of up to 1.5 m. The ash to sandstone interface is identified by a characteristic loss of signal strength in the underlying sandstone. Areas of interest containing animal skeletons are characterized by low amplitude, discontinuous reflectors encased within continuous high amplitude ash layers. Four distinctive GPR reflection characteristics identified within the ash beds correspond to the presence of animal skeletons or multiple skeletal remains as well as vertebrate and invertebrate ichnofossils (trace fossils). The four characteristic GPR signatures were mapped across the site. This study demonstrates that GPR is a suitable method for paleontological investigations in ash deposits. Also, the study proved successful in imaging the subsurface paleostratigraphy as well as identifying areas of interest that may contain the remains of prehistoric animal bone assemblages.

Acknowledgements

Thank you to my close family and friends for getting me through the years of work I have conducted as a graduate student. I would like to thank George Tsoflias for allowing me to pursue a degree and interest in geophysics within forensics, archaeology and paleontology, and Rolfe Mandel for introducing this research site and guidance with my thesis. A big thanks goes to Blair Schneider for being a mentor throughout my time at KU. I would also like to thank Rick Otto for being a great source of information about Ashfall Fossil Beds and allowing us to conduct the ground penetrating radar and a LiDAR survey. Thank you to Doug Walker for teaching and assisting me to acquire LiDAR data. Furthermore, I would like to thank John McQueeny and Cody Barnett for assisting in acquiring GPR data, and Jon Smith from the KGS for supplying the paleontological and ichnofauna history discovered at Ashfall. Thank you to the University of Kansas, Kansas Geological Foundation, and the Association for Women Geoscientists for financially supporting this research. Lastly, I would like to acknowledge that National Science Foundation EAR/IF-035445 funded acquisition of the GPR instrumentation.

Table of Contents

Figures and Tables

Chapter 1

1.1 Introduction

Ground Penetrating Radar (GPR) has successfully been utilized for subsurface imaging of human and animal remains at archaeological and forensic site investigations (Davis and Annan, 1989; Jol, 2009; Aziz et al., 2016; Damiata et al., 2013; Hansen et al., 2014; Schultz and Dupras, 2008; Zhao et al., 2018; Leucci et al., 2016). A similar field, paleontology, also contains the remains of fossilized bone deposits. However, there has been less research on the utilization of geophysical methods to detect fossil remains. Few studies that have employed GPR for paleontological purposes have reported with improving degrees of successful imaging. One of the earliest applications of GPR in paleontological studies was conducted by Gillette in 1994. Gillette attempted to image paleontological targets at New Mexico *Seismosaurus* site. Within Gillette's data, GPR anomalies were produced but the older imaging from the early GPR system is debatable. Main and Hammon (2003) used GPR at a known paleontological site at Big Bend National Park and Jones Ranch in Texas. They were able to successfully map out the site which led paleontologists to locate fossil remains. However, they were not able to detect any differences between the fossilized bone or wood within the rock that they were encased in. In Taimyr, Siberia, Grandjean et al. (2002) applied 900 MHz GPR antennas to image a thighbone and vertebrae bones belonging to a mammoth. Anomalies were recognized and used to locate scattered bones within the first few meters of permafrost (Grandjean et al., 2002). In addition, Makino and Miura (2004) successfully imaged prehistoric mammoth remains in the Siberian alluvial permafrost. With corresponding excavations, GPR anomalies within the survey area were discovered to be mammoth remains, one particularly a piece of backbone with meat still attached (Makino and Miaura, 2004). In 2012, Tinelli et al. successfully detected a nearly

complete fossilized skeleton of an Early Pliocene sirenian (a marine mammal). Most recently, detection of trace fossils (ichnofossils) in the form of human tracks and mammoth tracks were successfully imaged. The trace fossils were detectable because tracks were infilled which exhibits higher amplitude GPR reflections and possibly higher electrical permittivity as it holds more moisture than the surrounding substrate (Urban et al., 2019).

A recent study evaluated the capability of GPR to image modern bones and assessed the dielectric properties of the bones (Schneider and George, 2017; Schneider, 2017). Schneider (2017) noted GPR detection capability will vary in depositional settings in addition to a bone's size, shape, depth of burial, burial orientation, and weathering state. Understanding how bones are affected during fossilization and diagenesis (alteration after burial) is important when interpreting GPR data. Recent studies of fossilization and diagenesis provide insight on how those processes affect prehistoric vertebrate bones (Keenan, 2016). To understand the fossilization process, one must understand how bones are affected by chemical and physical composition of the specimen, climate, depositional setting, surrounding sediment, duration of burial (Lyman, 1994), and groundwater chemistry (Keenan, 2016). All of the variables that affect fossilization are rarely understood at a site, and that is the case at Ashfall Fossil Beds State Historical Park.

Ashfall Fossil Beds is the location of a mass-assemblage kill event associated with an eruption at the Bruneau-Jarbidge Caldera located in southwestern Idaho. Based on geochemical analysis that employed zircon (U-Pb) age dating, the eruption occurred around 11.86 ± 0.13 million years ago (Smith et al., 2018a). As the pyroclastic debris was falling over the Great Plains of the United States, approximately 30 cm of fine volcanic ash initially was deposited over

the region; however, over time, the watering hole and the surrounding region was mantled by over 2 m of fine ash (Figure 1.1).

Vertebrate animals perished over the months following the volcanic event that is recorded in the geologic record. The event caused mass mortality that ultimately led to the preservation of over 21 vertebrate taxa in the fine volcanic ash beds (Tucker et al., 2018; Appendix 1) (Figure 1.2).

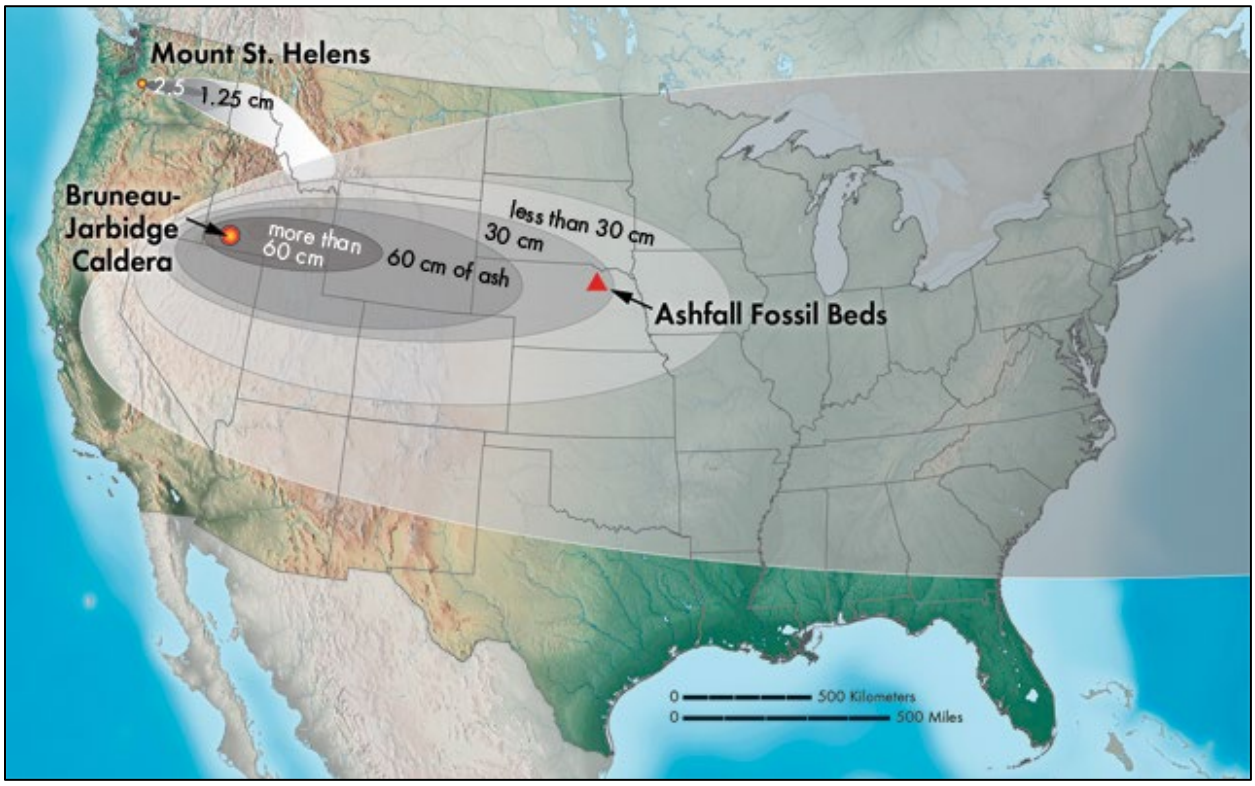

Figure 1. 1: The Bruneau-Jarbidge volcanic field is approximately 1,500 km from the Ashfall Fossil Beds site in Nebraska. The eruption sent fine volcanic ash over most of the United States. Image credit: University of Nebraska State Museum.

A)

B)

Figure 1. 2: **A**) Artist rendition of the Ashfall site prior to volcanic eruption, where a shallow pond is the source of water for animals. **B**) Artist Adrienne Stroup's rendition of what the pond looked like soon after the volcanic eruption. Images courtesy of the University of Nebraska State Museum.

Figure 1. 3: Mapped quadrants are outlined by a 3 x 3 m grid highlighted across the Hubbard Barn at Ashfall Fossil Beds (image created by Rick Otto).

Recent studies at Ashfall Fossil Beds focused mainly on identification of the animal skeletons and ichnofossils in the unexcavated portions of the ash beds at the Hubbard Barn (Figure 1.3). Applying a non-invasive geophysical technique, such as ground penetrating radar, would be beneficial to image the buried animal skeletons and ichnofossils. In principle, GPR imaging is well suited in low conductivity environments, such as volcanic ash, as there should be minimal signal attenuation. In other volcanic material, GPR is successful when applied to sites composed of volcanic medium encasing targets (Russell and Stasiuk, 1997; Pettinelli et. al, 2012). However, GPR has not been thoroughly tested in volcanic ash deposits, and it has not been used to detect bones in fine tuffaceous ash.

My research conducted at the Ashfall site applied high-frequency 500 MHz and 1 GHz GPR to non-invasively detect and image buried faunal remains and ichnofossils (or trace fossils) in the subsurface. The primary goal of this thesis is to assist paleontologists and ichnologists locate faunal remains and ichnofossils within the Hubbard Barn. The main research objectives are as follows:

- Determine if GPR can successfully image ash layers using 500 MHz and 1 GHz frequency antennas.
- Determine if GPR can detect stratigraphy and identify signatures of ichnofossils within the ash beds.
- Identify characteristic GPR signatures related to the presence of buried vertebrate skeletal remains.
- Interpret the GPR signatures and map them across the unexcavated section of the site.

- Compare the GPR imaging capabilities of the 500 MHz and the 1 GHz data for the search of faunal targets and other paleostratigraphic features.

Background information on the paleontology of the Ashfall Fossil Beds Site as well as previous research is summarized in Chapter 1, along with relevant information about GPR theory and principles that will facilitate the understanding of terminology and concepts in the subsequent chapters. The second chapter of my thesis evaluates the effectiveness of 1 GHz GPR frequency data for imaging the skeletons of large animals (barrel-bodied rhinoceros) buried in ash at the study site. The third chapter analyzes GPR response to the ash layers vs. the underlying sandstone, and maps the ash-sandstone contact across the site. Chapter 4 assesses the use of GPR for imaging the burrow of a scavenging animal. The fifth chapter summarizes and evaluates the characteristic GPR anomalies associated with the presence of buried animal skeletons and other paleontological features in the ash beds. The final chapter presents concluding remarks on the effectiveness of GPR for paleontological investigations at Ashfall Fossil Beds Site.

1.2 Site Description

Ashfall Fossil Bed State Historical Park is located 15 km north of the town of Royal in northeastern Nebraska (Figure 1.4). In 1953, the University of Nebraska State Museum (UNSM) collected a *Teleoceras major* (barrel bodied rhinoceros) skull and jaws from the Ashfall hillside (Voorhies, 1985). While engaged in geological mapping, Voorhies recorded the first intact *Teleoceras major* skeleton eroding out of an outcrop at the site. The skull proved to be articulated with an entire skeleton of a juvenile rhino and to be associated with numerous other complete skeletons (Voorhies, 1985). During a 1977 field season, 12 rhinoceros and three horse skeletons were collected from an area of only few tens of square meters (Voorhies, 1985). From 1978-1979, excavations funded by the National Geographic Society led to the discovery of 120 skeletons from multiple vertebrate taxa (Table A1 and Figure 1.5). During that time, the Ashfall Fossil Beds State Park was opened to the public to display the fossil discoveries (Tucker et al., 2014). In 2009, the Hubbard Family Rhino Barn was opened to the public and currently has active palaeontologic excavations.

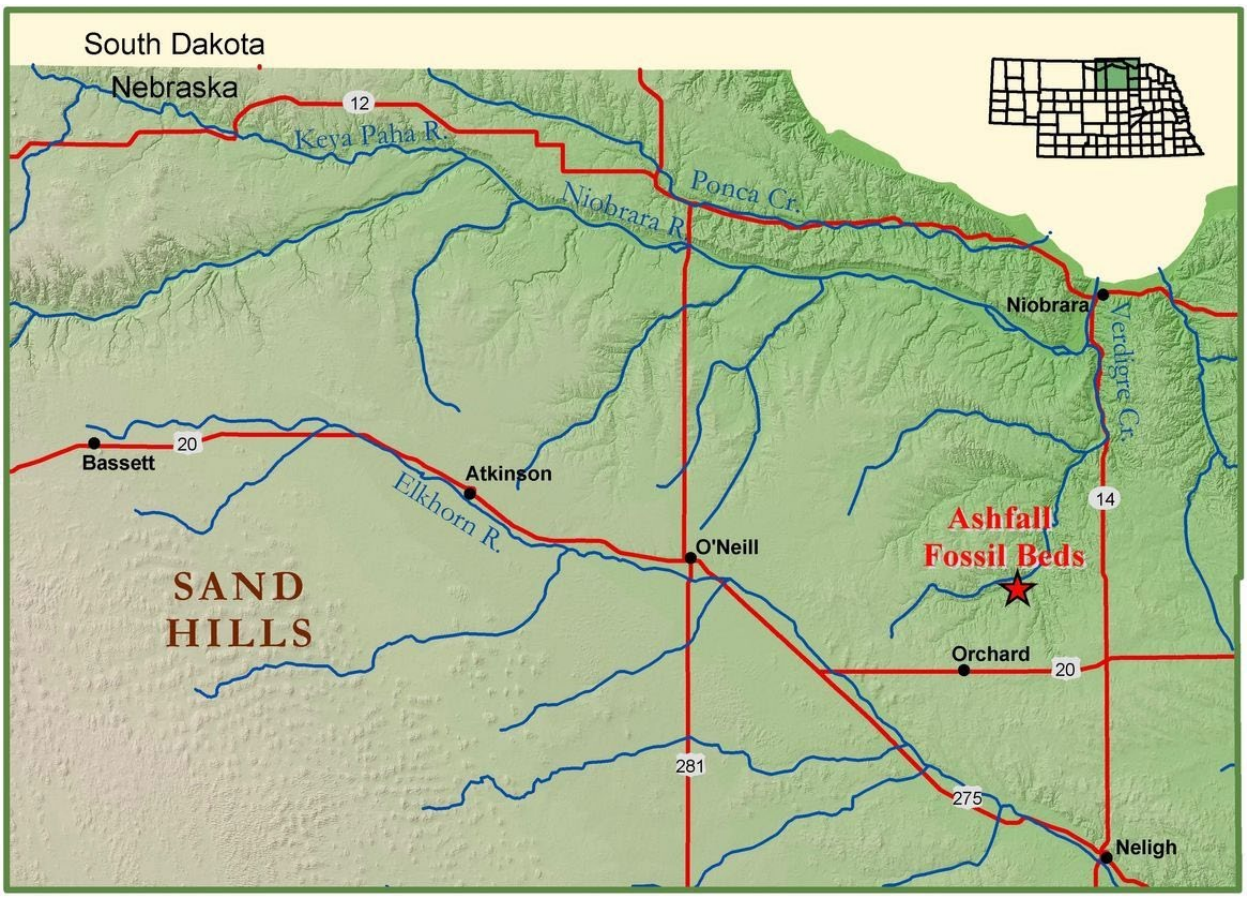

Figure 1.4: Map showing the location of Ashfall Fossil Bed State Historical Park (Voorhies et al., 2016).

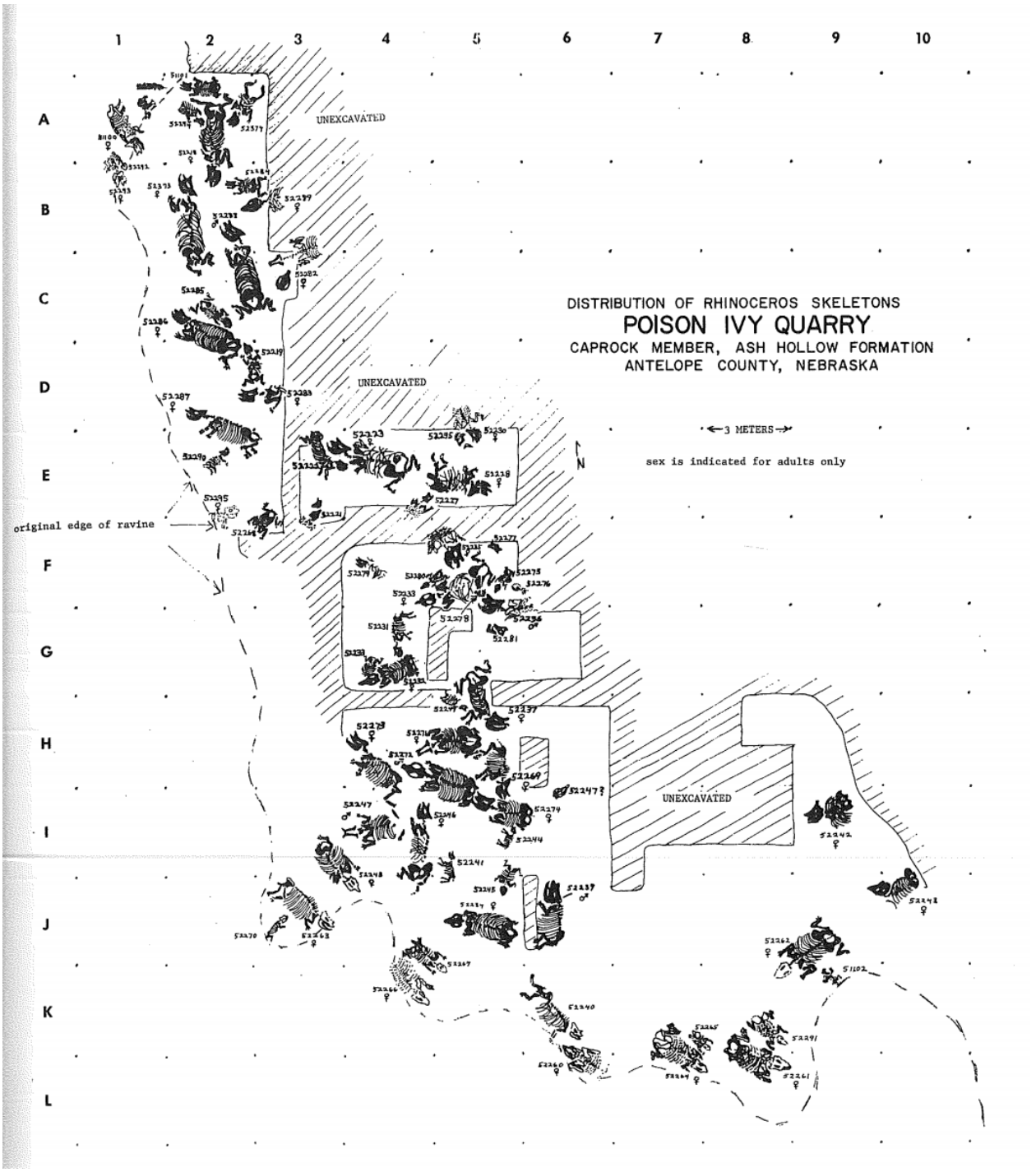

Figure 1.5: Distribution of rhinoceros skeletons from preliminary paleontological excavation funded by National Geographic Society in 1978 (Voorhies, 1985).

1.2.1 Geologic Setting

The Ashfall Fossil Beds site consists of well-preserved vertebrate animal remains from a late Miocene mass mortality event (Tucker et al., 2014). There is a paleodepression at the site, interpreted as a watering hole, which contains the vast majority of the fossils uncovered to date. The fossilized animal bones within and around the paleodepression are mantled by 2.5-3.0 m of ash (Tucker et al., 2014). Moving away from the paleodepression, the depth to the ash-sandstone contact decreases to approximately 1 m below the ground surface throughout the unexcavated site (Smith et al., 2018a).

In Nebraska, the Miocene-age Ogallala Group mostly consists of the two formations, Valentine and Ash Hallow formations, both of which are exposed at Ashfall. The Ash Hallow Formation of the Ogallala Group is comprised of the ash deposits found at Ashfall Fossil Beds (Figure 1.6). The Valentine Formation consists of fluvial sand and gravel, silty sand, and silt, and is divided into the following four members (from oldest to youngest): Cornell Dam, Crookston Bridge, Devil's Gulch, and Burge members (Tucker et al., 2014). The Crookston Bridge and Devil's Gulch members occur at Ashfall Fossil Beds. The Ash Hallow Formation is further divided into the Cap Rock and Merritt Dam members (Skinner et al., 1968; Skinner and Johnson 1984; Tucker et al., 2014). The *Konservat-Lagerstätte* ash layer, estimated to be about 2.5-3 m in thickness, is found within the Cap Rock Member (Skinner and Johnson 1984; Tucker et al., 2014). At Ashfall Fossil Beds, the volcanic ash deposits containing the faunal remains fit the criteria of *Konservat-Lagerstätte.* Adolf Seilacher introduced the term *Konservat-Lagerstätte* and defined it as deposits with exceptional preservation of fossilized organisms and/or ichnofossils (Seilacher, 1970).

1.2.2. Ash Hollow Tuff: Paleontology and Ichnology

Smith et al. (2018b) identified three distinctive "zones" within the *Konservat-Lagerstätte* ash: the Recovery Zone, the Dead Zone and the Skeleton Zone. The lowest zone is the Skeleton Zone, which is approximately 30 cm thick and mantles the sandstone unit (part of the Cap Rock Member). The Dead Zone, which is about 2 m thick, overlies the Skeleton Zone and is devoid of intact fossils. Overlaying the Dead Zone is the Recovery Zone, which contains scattered fossils (Figures 1.6).

Previous excavations have removed the overburden inside of the barn, leaving approximately one meter of the volcanic ash remaining above the sandstone contact. This study will be primarily imaging within the Dead and Skeleton Zone but not in the Recovery Zone. The depth to sandstone varies away from the center of the paleodepression within the Hubbard Barn. Figure 1.6 and Figure 1.7 shows the stratigraphy within the Hubbard Barn. Additional information on the skeletal remains of the 21 invertebrate taxa within the ash and sandstone is in Appendix Table A2.

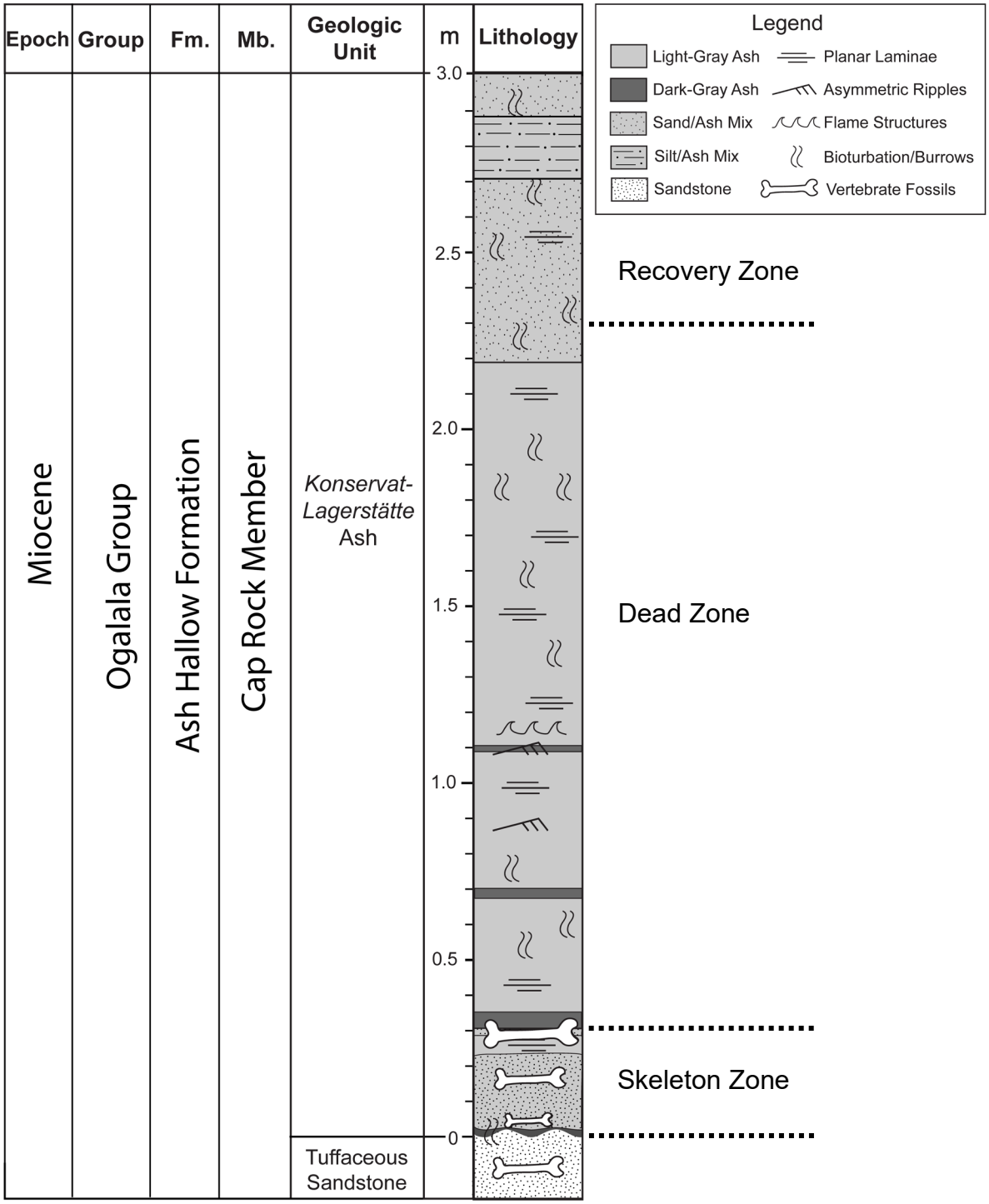

Figure 1. 6: Stratigraphic column within the Hubbard Barn at Ashfall Fossil Beds (modified from Voorhies [1985], Tucker et al. [2014], and Smith et al. [2018a, 2018b]). Refer to section 1.2. for descriptions of the three zones identified in the ash column.

1.2.2.1 Dead Zone

Located about 0.30 to 2.20 m above the sandstone, the Dead Zone was originally considered a portion of the volcanic ash devoid of fossils. However, recent studies revealed that the Dead Zone contains an assemblage of ichnofossils indicative of biodiversity and scattered bones (Smith et al., 2018b). Currently, the Dead Zone contained within the interior of the Hubbard Barn is being excavated by paleontologists and stratigraphers.

The Dead Zone consists of beds of light and dark gray ash with planar laminae and flame structures, plus algal mats, and biogenic features (Figure 1.6). Smith et al. (2018b) recorded traces of fauna such as rhizoliths, and larger biogenic features such as subvertical burrows associated with carnivorous animals. Tucker et al. (2014) observed a burrow 16 cm in diameter containing a rodent tooth, as well as other burrows with faunal remains. Also, vertebrate canid tracks likely belonging to one of the six “dog” species have been identified within the Dead Zone, along with coprolites and fossilized ant nest (Tucker et al., 2014; Smith et al., 2018b).

1.2.2.2 Skeleton Zone

The Skeleton Zone is 30-40 cm thick and mantles the underlying tuffaceous fine silty sandstone. It is composed primarily of the volcanic ash, however, some of the sediment from the sandstone unit below has inter-mixed into the volcanic ash at the base of the Skeleton Zone. Three distinctive horizons of vertebrate taxa occur in the Skeleton Zone (Figure 1.7) (Tucker et al., 2014; Smith et al., 2018 b). The oldest and deepest horizon (a_1) is about 10 cm and consists of small taxa (reptiles, birds, and moschids) above a dark gray ash layer. It is likely that the fauna in level a_1 died hours after the airfall pyroclastic event (Tucker et al., 2014). The middle horizon (a_2) contains medium-sized animals, such as camelids (camels) and equids (horses) that probably perished a few days after the pyroclastic event. The upper horizon (a_3) consists of reworked ash (slopewash) and contains skeletal remains of large animals, such *Teleoceras major* (barrel bodied rhinoceros) that perished weeks or months after the volcanic eruption (Voorhies, 2016). The skeletal remains of the large animals often show evidence of *hypertrophic osteopathy* (Marie's Disease or Bamberger-Marie Disease), an abnormality characterized by frothy, rough, and/or patchy bone growths on the surface of normal bones (Voorhies et al., 2016; Tucker et al., 2014).

The remains of smaller animals near the base of the "Skeleton Zone" tend to be less intact than the remains higher in the bone bed. In many cases, the bones of small animals are flattened, and elements such as skulls are missing. By contrast, the skeletal remains of the barrel-bodied rhinos typically are complete and articulated (Voorhies, 2006; Tucker et al., 2014). In addition, ichnofossils such as rhizoliths, small to large size animal burrows, horizontal ant nets hubs and some coprolites (Smith et al., 2018b).

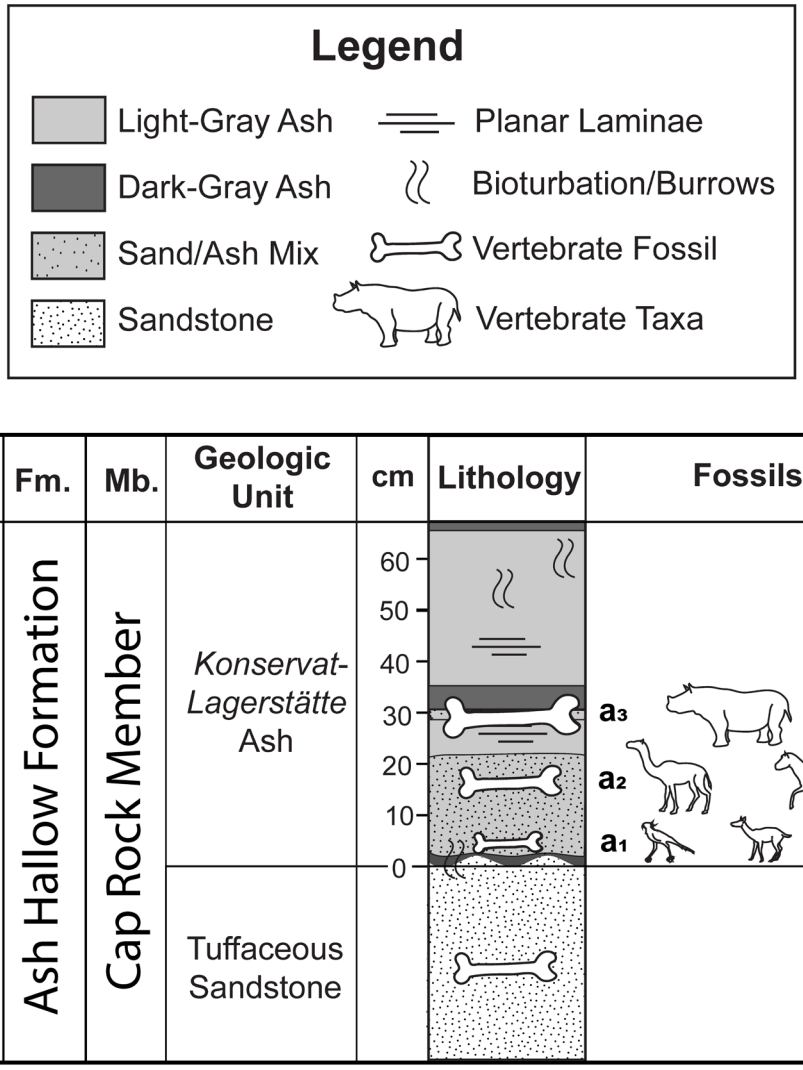

Figure 1. 7: Stratigraphic column of the lower portion of the volcanic ash deposit showing the three distinctive horizons of vertebrate taxa remains (modified from Voorhies [1985], Tucker et al. [2014], Voorhies et al. [2016], and Smith et al. [2018a] and based on illustrations by Mark Marcuson).

1.2.2.3 Sandstone of the Cap Rock Member

At Ashfall Fossil Beds, tuffaceous fine silty sandstone comprises the lower part of the Cap Rock Member of the Ash Hollow Formation (Fig. 1.6). The exposed portion of the tuffaceous fine silty sandstone is approximately 1.5 m thick and occurs immediately below the "Skeletal Zone" (Tucker et al., 2014). An array of vertebrate and invertebrate fossils has been exhumed during excavation at the site (Voorhies et al., 2016, Tucker et al., 2014). Paleontologists discovered over 80 fossilized taxa within this sandstone unit of the Cap Rock Member (Appendix-Table A2).

Figure 1. 8: Image of GPR data being collected over the present-day surface of ash found in the Hubbard Barn. Image courtesy of Rick Otto.

1.3 Methods

1.3.1 Ground Penetrating Radar Theory

Ground penetrating radar (GPR) is a non-invasive high frequency method for imaging the subsurface. The electromagnetic (EM) waves generated by the typical GPR instrumentation can range in frequency from 10-1000 MHz. The principles of EM wave propagation are described by Maxwell's Equations (Balanis, 1989). The transmitting antenna emits a pulse of radar waves in the frequency ranges of 10-1000 MHz. These radar waves are reflected back to the receiving antenna as they encounter subsurface materials with different relative permittivity values (Davis and Annan, 1989). Relative permittivity is defined as the permittivity of a given material relative to that of the permittivity of a free space and is directly related to the velocity of propagation of the GPR wave (equation 1).

$$(1)\ v = \frac{c}{\sqrt{\varepsilon_r}}$$

where v is the velocity of propagation, c is the speed of light (0.3 m/ns) and ε_r is the relative permittivity.

Within paleontological studies, GPR surveys commonly employ varying frequencies, ranging as 150 MHz to 1 GHz, to identify vertebrate megafauna fossils within the shallow subsurface (Lukjanov et al., 2007; Tinelli et al., 2012; Udphuay et al., 2020). Lower frequencies image to greater depths but at the cost of reduced resolution (Lukjanov et al., 2007). Higher frequencies image the shallower subsurface but provide higher resolution imaging (Udphuay et al., 2020). Higher frequencies (defined here as greater than 200 MHz) have shorter wavelengths and are used primarily to map the shallowest subsurface layers (decimeters to a few meters). Lower frequencies (defined here as less than 200 MHz) have longer wavelengths and typically

image deeper into the subsurface, up to several meters or 10s of meters in suitable geologic media. Radar wavelengths are related to both the wave frequency and velocity of propagation as defined in equation 2.

$$(2)\ \lambda = \frac{v}{f}$$

where λ is the wavelength, v is the velocity of propagation and f is the frequency.

A second factor that impacts GPR imaging capabilities is the electrical conductivity (σ) of the subsurface layers. GPR surveys are typically best suited in media with low electrical conductivity, such sandy soils, dolomite, limestone, and sandstone. Those mediums are considered low attenuation environments for radar wave propagation (Table 1.1). Attenuation (α) is defined as the absorption of a wave's energy as it travels through a medium (Jol, 2009) (see equation 3).

$$(3)\ \alpha = \omega\sqrt{\mu\varepsilon}\left(\frac{1}{2}\left[\sqrt{1+\left(\frac{\sigma}{\omega\varepsilon}\right)^2}-1\right]\right)\ \left(\frac{Np}{m}\right)$$

where α represents the attenuation coefficient, ω is the angular frequency, μ is the magnetic permeability, ε is the electrical permittivity, and σ is the electrical conductivity. By contrast, GPR waves will attenuate rapidly in saline water bodies, silty soils, shales, and mudstones, because of the higher electrical conductivity values (equation 3 above). At Ashfall Fossil Beds, GPR is expected to image through the silica rich, low conductivity volcanic ash layers, but signal will attenuate rapidly in the underlying higher electrical conductivity tuffaceous silty sandstone.

Material	ε_r (relative permittivity)	σ (mS/m) (electrical conductivity)	V (m/s) (Velocity)	α (dB/m) (Attenuation)
Air	1	0	.3	0
Distilled water	80	0.01	0.033	0.002
Fresh water	80	0.5	0.033	0.1
Sea water	80	3000	0.01	10^3
Dry sand	3- 5	0.01	0.15	0.01
Saturated sand	20-30	0.1-1.0	0.06	0.03-0.3
Limestone	4-8	0.5-2.0	0.12	0.4-1
Shales	5-15	1-100	0.09	1-100
Silts	5-30	1-100	0.07	1-100
Clays	5-40	2- 1000	0.06	1-300
Granite	4-6	0.01-1.0	0.13	0.01-1
Dry salt	5-6	0.01-1.0	0.13	0.1-1
Ice	3-4	0.01	0.16	0.1

Table 1.1: Medium relative permittivity, electrical conductivity, EM velocity, and attenuation through common subsurface materials at a signal frequency of 100 MHz (modified from Annan, 2003).

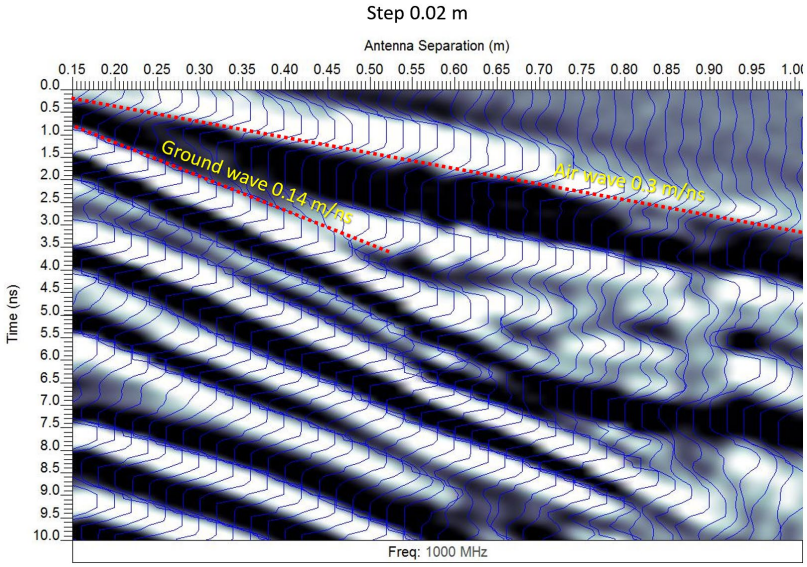

Figure 1. 9: Common Midpoint profile (CMP) used to estimate of GPR wave velocity of propagation. The interpreted direct air wave and direct ground wave are identified by dotted lines.

In order to determine the velocity of propagation at Ashfall Fossil Beds, a Common Midpoint (CMP) survey was collected. A CMP survey is used to estimate the radar signal velocity verses true depth in the ground by incrementally increasing transmitter and receiver antenna separation and recording corresponding wave arrivals (Figure 1.9). Observation of the direct ground wave arrivals and the reflected wave arrivals allow the estimation of subsurface velocities of GPR waves (Annan, 2003). The CMP survey was conducted using the 1 GHz frequency in Quadrant Q (Figure 1.8). Uniform environmental conditions provided by the enclosing structure of the Hubbard Barn allow the use of a single CMP survey for estimation of GPR wave velocity across the entire site.

Using time – distance observations in figure 1.9 yields a direct ground wave velocity of 0.14 m/ns, which is in the range of expected velocity values for volcanic materials (0.01 m/ns to 0.15 m/ns) (Russell and Stasiuk, 1997; Cagnoli and Russell, 2000). Using this information, the value of the relative permittivity of ash was calculated to be 4.6, which agrees closely to the expected material values for volcanic material, which is 5-6 (Oguchi et al., 2009). The estimated radar wave velocity along the known signal frequency and equation 2, are used to calculate of the GPR signal wavelength and obtain an estimate of the resolution of the data. Resolution is the ability of the GPR signal to distinguish two objects that are close to one another. GPR wave resolution is equal to one quarter of its dominant wavelength (Davis and Annan, 1989). The 1 GHz data has a wavelength of 0.14 m and the 500 MHz data has a wavelength of 0.28 m. Therefore, the 1 GHz data has a resolution of 3.5 cm, and the 500 MHz data has a resolution of 7 cm.

1.3.2 Ground Penetrating Radar Data Acquisition

The GPR survey area is located within the unexcavated portion of the Hubbard Rhino Barn and covers approximately 25 x 15 m. The area was subdivided into quadrants, and the average size of each quadrant was 18 x 6 m (as indicated in Figures 1.8, 1.10 and 1.12). However, a few of the quadrants were partially excavated or unavailable for the GPR survey. GPR data were acquired over the partially excavated ash deposits (Figure 1.11) ranging in height from approximately 0.6 m to 1.5 m above the paleodepression surface.

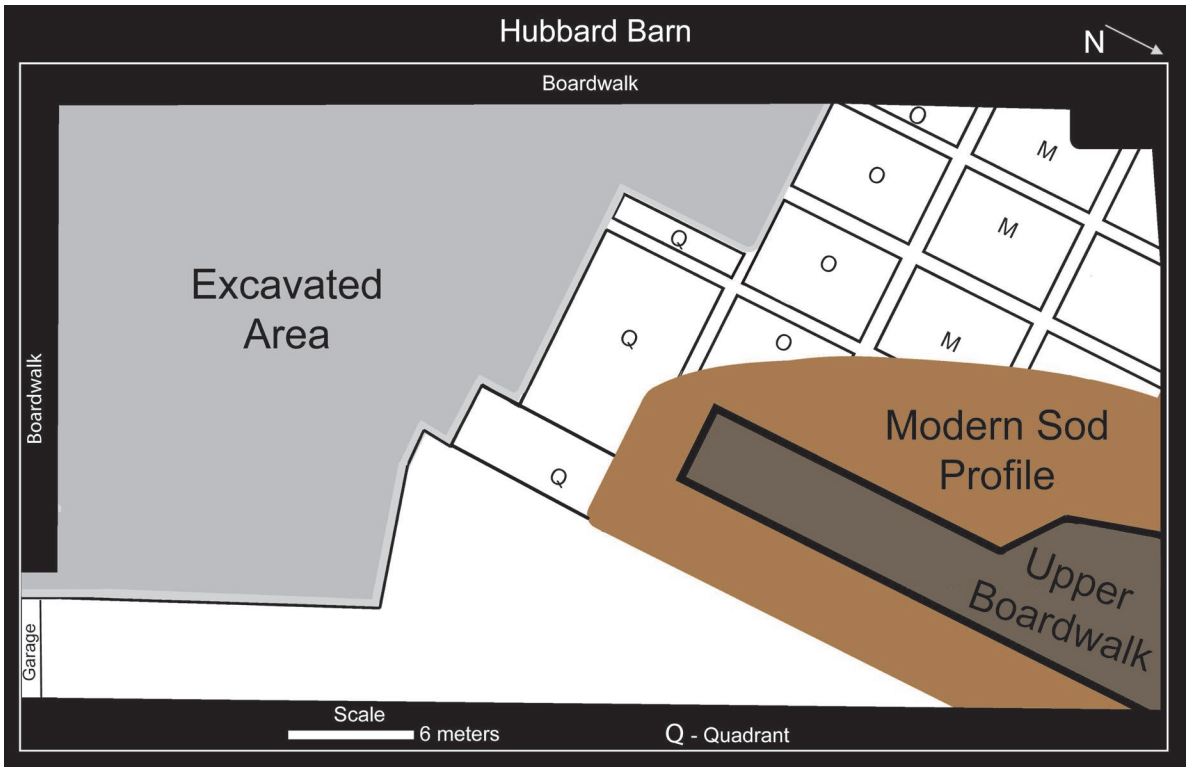

Figure 1.10: Schematic of the Hubbard Barn showing the excavated area and the unexcavated quadrants. Quadrants labeled by the letters Q, O, M identify the area of contiguous GPR line collection.

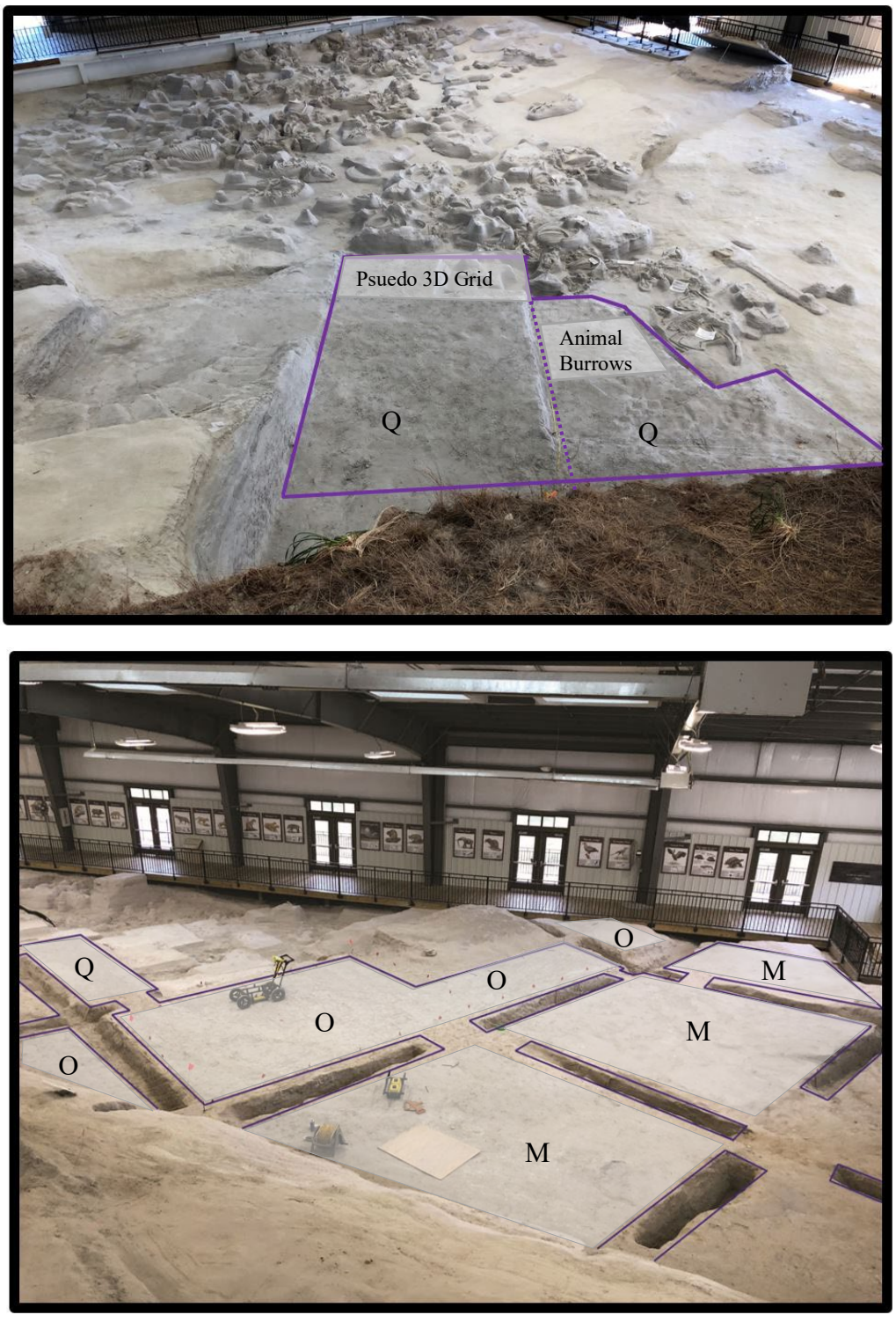

Figure 1. 11: GPR survey area and outlined unexcavated quadrants within the Hubbard Barn. Letters identify quadrants of contiguous GPR data line collection. Images taken on upper boardwalk shows areas of excavation and unexcavated quadrants from an aerial view of the site.

Quadrant Name	Number of Inlines	Number of Crosslines	Line Spacing-Inline (m)	Line Spacing-Crossline (m)
Quadrants O	24	7	0.2	1
Quadrants M	24	3	0.2	Varied
Pseudo 3D Grid (Q21)	13	1	0.05	-
Quadrant Q 21	9	1	0.1	-
Quadrant Q 20	8	0	0.1	-

Table 1.2: List of quadrants along with the total number of GPR lines collected throughout Ashfall Fossil Beds. GPR line locations are shown in Figures 1.14.

GPR surveying at Ashfall Fossil Beds was completed in two stages (Table 1.2). An initial investigation conducted in June 2019, as described in Chapter 2, evaluated the use of the Sensors and Software PulseEKKO Pro GPR system with 500 MHz and 1 GHz antennas for imaging ash deposits and detecting large animal skeletons at a location of a known buried barrel-bodied rhino. Following the successful initial investigation, the remainder of the unexcavated site was surveyed by GPR in September 2019, as described in Chapters 3 and 4.

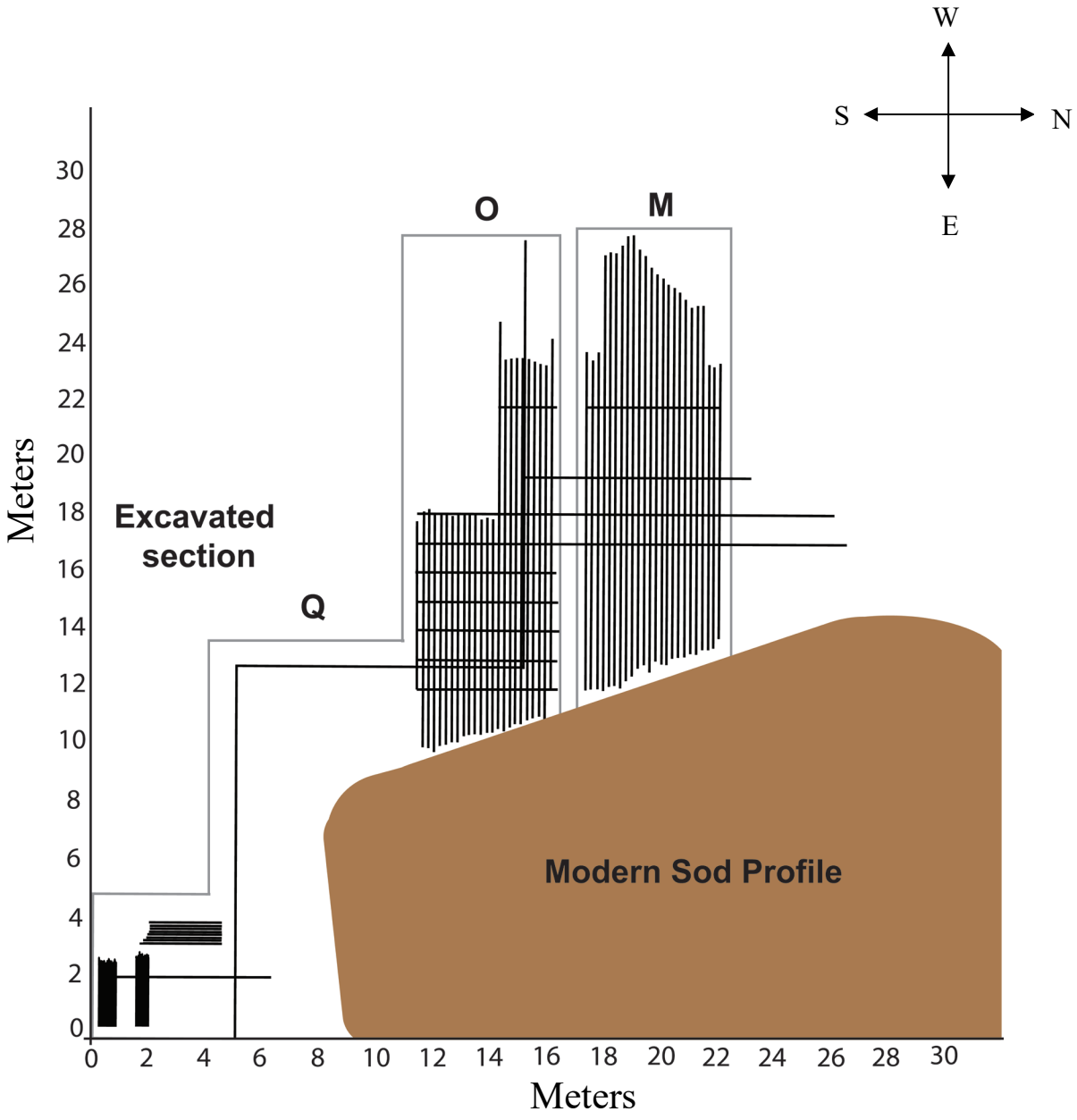

Figure 1. 12: Arial map view of GPR line grid in the unexcavated portion within the Hubbard Rhino Barn at Ashfall Fossil Beds. A total of 173 lines were acquired, with 154 closely parallel oriented lines and 19 orthogonal intersecting lines. The preliminary GPR surveys were collected in the lower southeast corner or near the origin of the map.

1.3.3 GPR Data Processing

GPR data were processed to reduce noise, enhance signal, and construct accurate images of the subsurface. Data were processed using the Matlab based MatGPR software (Tzanis, 2016). The processing steps applied to the data for each quadrant were as follows: (1) adjusted trace time position to correct for instrument drift, (2) applied a band-pass frequency filter between 500-2000 MHz for the 1 GHz frequency data and between 250-1000 MHz for the 500 MHz data, and (3) employed an F-K Stolt migration using a velocity of 0.14 m/ns estimated by the CMP survey. All GPR processing parameters are summarized in Table 1.3 and 1.4. The processed data were imported to IHS Kingdom® for interpretation. The display color bar in Kingdom suite was adjusted (clipped) to help delineate stratigraphy and weak reflections.

1 GHz - Quadrant Name	Adjustment signal		Band pass-Low (Hz)	Band pass-High (Hz)
	Sample #	ns		
Quadrant O	26	2.6	500	2000
Quadrant M	24	2.4	500	2000
3D Survey-Quad Q21	23	2.2	500	2000
Quadrant Q21	23	2.2	500	2000
Quadrant Q20-Animal Burrow	22	2.2	500	2000
Ash to Sandstone Contact	-	-	500	2000

Table 1. 3: List of the 1 GHZ frequency GPR lines with processing parameters.

500 MHz - Quadrant Name	Adjustment signal		Band pass-Low (Hz)	Band pass-High (Hz)
	Sample #	ns		
Quadrant O	33	6.4	250	1000
Quadrant M	25	4.4	250	1000
Quadrant Q21	24	4.8	250	1000
Quadrant Q20-Animal Burrow	20	5.6	250	1000
Ash to Sandstone Contact	-	-	250	1000

Table 1. 4: List of 500 MHz frequency GPR lines with processing parameters.

Chapter 2: 3D GPR Imaging of Animal Remains

2.1 Introduction

During the initial GPR investigation conducted at Ashfall Fossil Beds, an area that contained the potential remains of a large animal was identified. Because that area was about to be excavated by paleontologists, it provided an opportunity to ground truth the capability of GPR to image animal remains buried in volcanic ash. A partially exposed jaw protruding from the ash deposit indicated the approximate location of the remains of a skeleton. At that location, the ash deposit was about 70 cm thick above the mantled sandstone.

2.2 Methods

A dense grid of radar profiles was acquired to assess the imaging capabilities of the GPR method. Figure 2.1 shows the location of the grid of the GPR lines in relation to the partially exposed jaw of a barrel-bodied rhinoceros (called Rae). The approximate dimensions of the 3D radar survey area are 0.70 m in width by 2.30 m in length. The psuedo 3D GPR grid consists of 13 densely spaced parallel lines acquired at 5 cm spacing between lines, with 1 cm trace spacing using the 1 GHz frequency GPR system. The GPR lines are oriented perpendicular to the exposed remains of a suspected rhinoceros (Figure 2.2a). A detailed image of the exposed jaw is shown in Figure 2.2b. The GPR lines were processed following the methods described in Chapter 1.3.3. After processing, the GPR lines were imported into Kingdom Suite to create a pseudo 3D grid for interpretation.

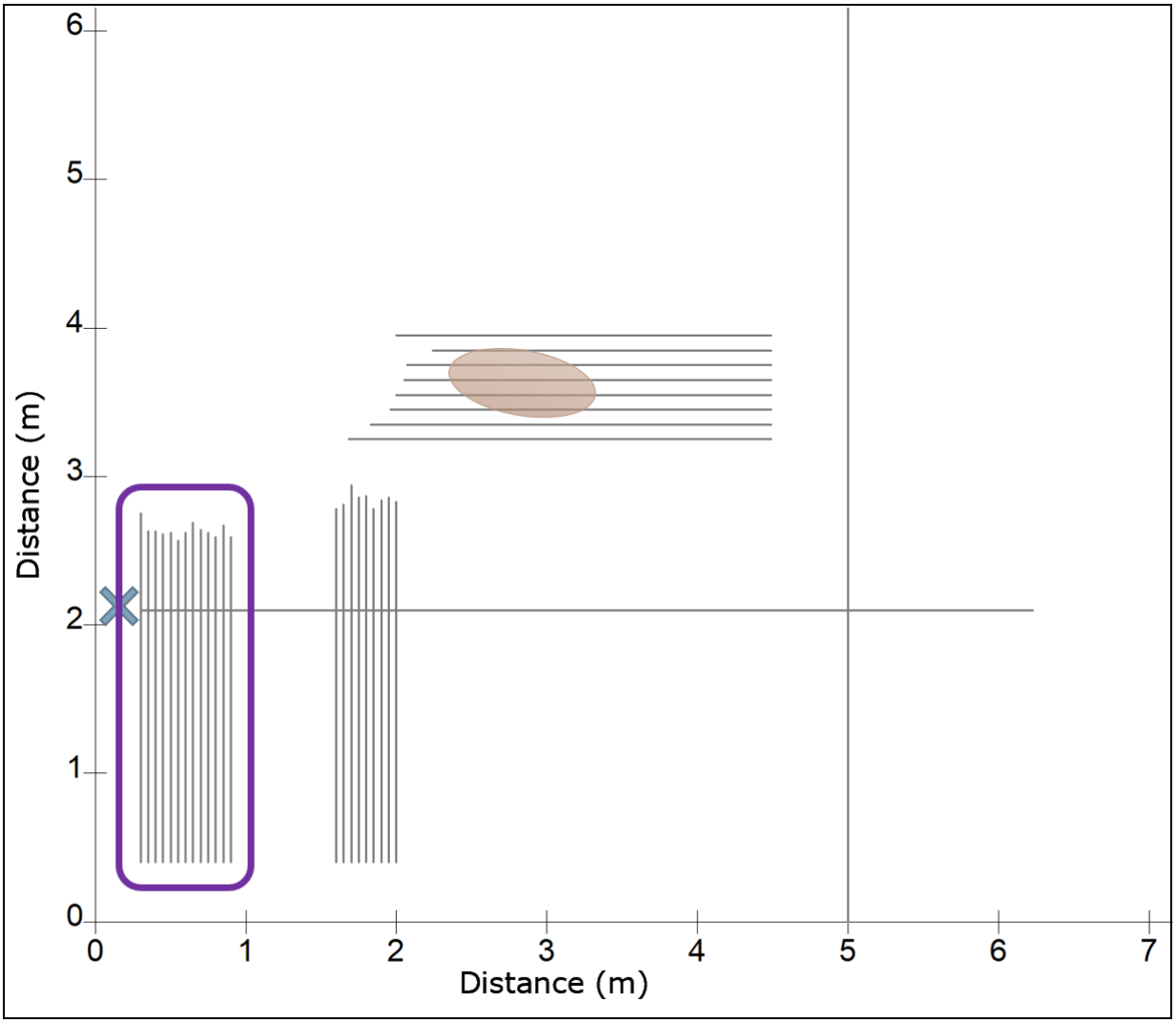

Figure 2. 1: Location map of the pseudo 3D GPR survey grid (outlined by the purple box) containing the partially exposed jaw (marked by the blue X) of a female barrel-bodied rhinoceros, called Rae. This survey is located in the southwest corner of the Hubbard Barn (refer back to the southeastern portion of Figure 1.11).

(A) **(B)**

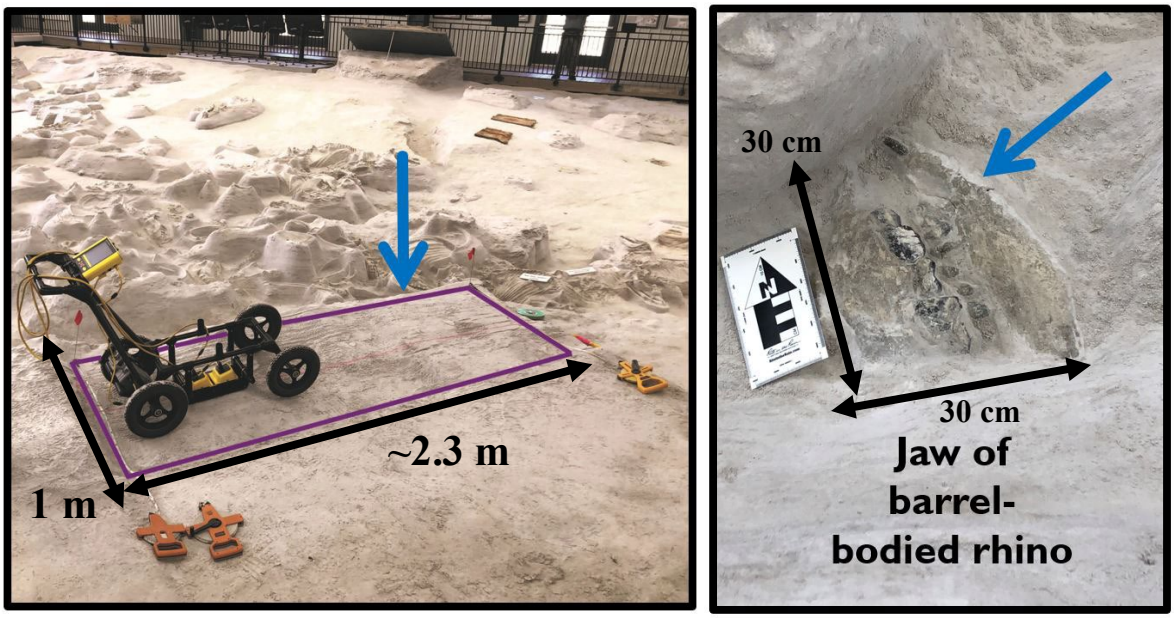

Figure 2. 2: (**A**) Outlined area of the GPR grid acquired over the suspected remains of a barrel-bodied rhinoceros. (**B**) Overhead photograph of the exposed jaw of the rhinoceros. The blue arrow marks the location of the exposed jaw.

2.3 Results

2.3.1 GPR Profiles

Figures 2.6-2.9 show interpreted GPR profiles acquired before excavation began over Rae's jaw, neck, shoulder, and ribcage. The horizontal axis represents distance (m) along the profile, and the vertical axes are two-way travel time (ns) and depth (m). Time is converted to depth using a constant velocity of 0.14 m/ns determined from the CMP survey. The GPR data show high amplitude, mostly continuous reflections corresponding to the volcanic ash layers that mantle the sandstone. However, the continuity of the ash layers is disrupted in the volcanic ash layers directly above the sandstone contact by localized lower amplitude, discontinuous reflections. Data amplitude decreases rapidly deeper in the radar profile as the signal enters the underlying sandstone, which has higher attenuation rates (> 70 cm depth). Uninterpreted images are in Appendix Figures A1-A4.

2.3.2 Excavation of 3D GPR Survey Area

Excavation of the GPR survey grid confirmed the components and location of the skeleton. The exposed, mostly intact skeleton of a female barrel-bodied rhino, Rae, occupies an area approximately 1.5 x 2.0 m (Figures 2.3 and 2.4). Discoloration of the bones has occurred because excavation exposed them to air. It is likely that a rib bone and other bones scattered around the skeleton of the rhino are from different animals (Rick Otto, personal communication, 2020). Scavenging animal or natural depositional processes, such as sheetwash, may have deposited those bones. Alternating beds of light and dark ash can also be seen on the exposed face of the ash in Figure 2.4.

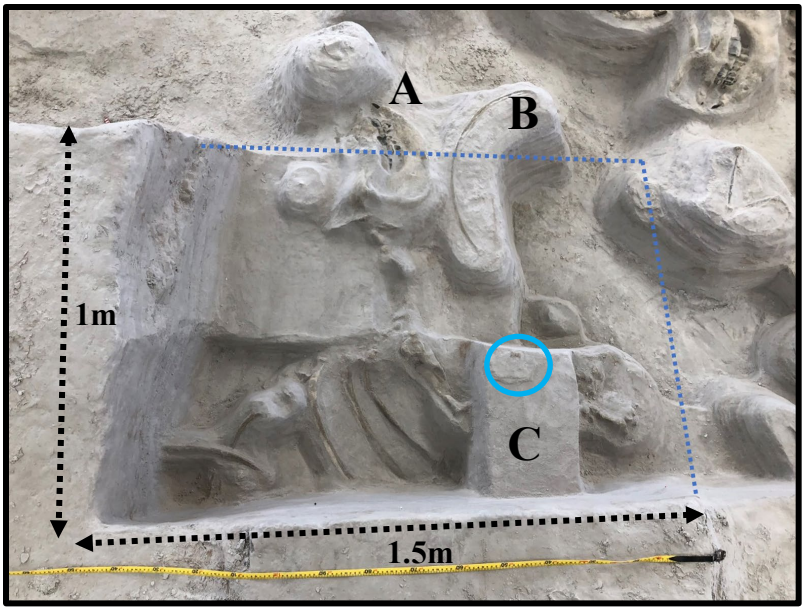

Figure 2. 3: Overhead photograph of the excavated portion of the skeletal remains of a female barrel-bodied rhinoceros. The exposed jaw is marked by **A,** and a rib bone is marked by **B**. The GPR survey was conducted within the area of the blue dotted lines. (**C**) Scattered knuckle bone is found 20 cm above the skeletal remains of the rhinoceros. This knuckle bone does not belong to the rhinoceros below and was most likely deposited here by sheetwash.

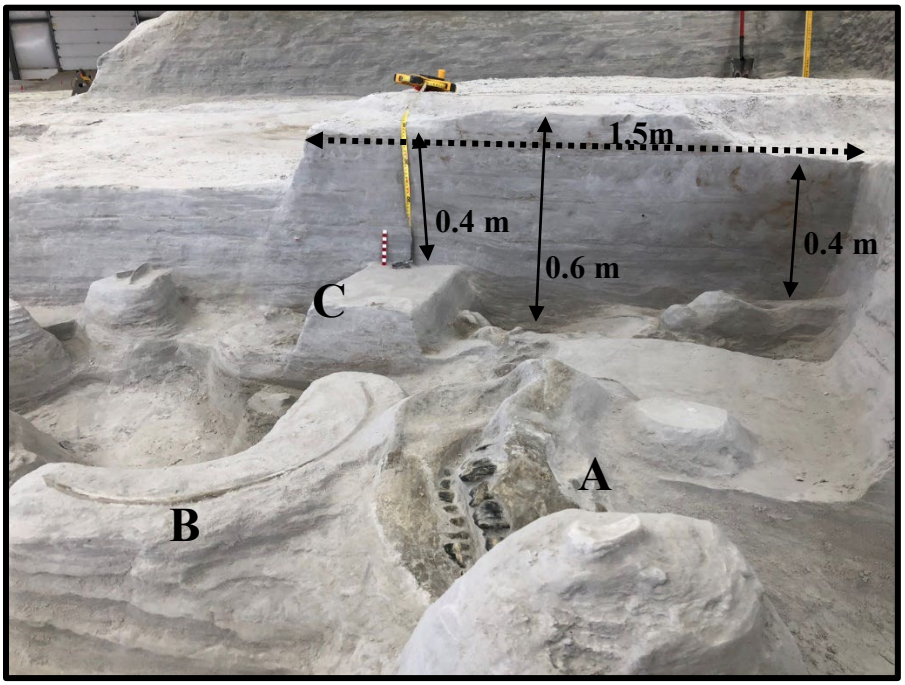

Figure 2. 4: Exhumed region with an isolated rib bone (**B**) alongside the (**A**) exposed rhinoceros' skeleton, and another animal's knuckle bone (**C**). Ash stratigraphy, 60 cm thick, can be seen along the exhumed region above.

2.4 Discussion

2.4.1. GPR Survey Interpretation

Interpreted GPR profiles are correlated to the pseudo 3D grid containing the excavated rhinoceros, Rae, presented in Figure 2.2 to 2.4. Low amplitude, discontinuous reflections in the GPR data spatially correlate with Rae's excavated skeleton, which is confined to the Skeleton Zone resting over the sandstone (Figures 2.6-2.10). There is a continuous GPR reflection atop the skeleton that is likely marking the transition into the Dead Zone (upper 30 cm of GPR data) that contains ash layers.

There is a large loss of radar energy as it encounters the underlying sandstone unit, which is known to occur at a depth of 65-75 cm in an exposure. The loss of GPR signal amplitude in the sandstone is consistent with the higher electrical conductivity resulting in signal attenuation. Therefore, the boundary from strong amplitudes to weaker amplitudes is interpreted as the location of the ash-sandstone contact. Above the ash-sandstone contact, areas of amplitude loss are recorded within the continuous high amplitude GPR reflections. These areas of amplitude loss are interpreted as buried bones occurring within the ash. Schneider (2017) observed large bones of modern mammals buried in the sand caused strong GPR scattering seen as hyperbolas (diffractions) in the data. However, the amplitude decreased as the weathering of bones increased, which is similar to the results of this study. However, in this study, GPR images of fossilized bones do not show diffractions and, therefore, do not indicate strong electrical property contrast with the encasing volcanic ash. Instead, the fossilized bones are imaged as discontinuous and low amplitude reflections within surrounding strong and continuous reflections of the ash deposit. Hence, fossilization of bone appears to reduce the amplitude of the GPR signal.

Figure 2.10 shows a 3D perspective of the interpreted ash layer, the contact with the sandstone, and the location of the buried rhinoceros. GPR images ash layers as strong reflections and differentiates ash deposits from the sandstone based on signal amplitude loss. This can be seen in the Figures 2.6 -2.9 as the sandstone contact is mapped by distinctive signal loss around 45-75 cm. This interpretation allows mapping of the thickness of the ash deposits and topography of the sandstone around the site.

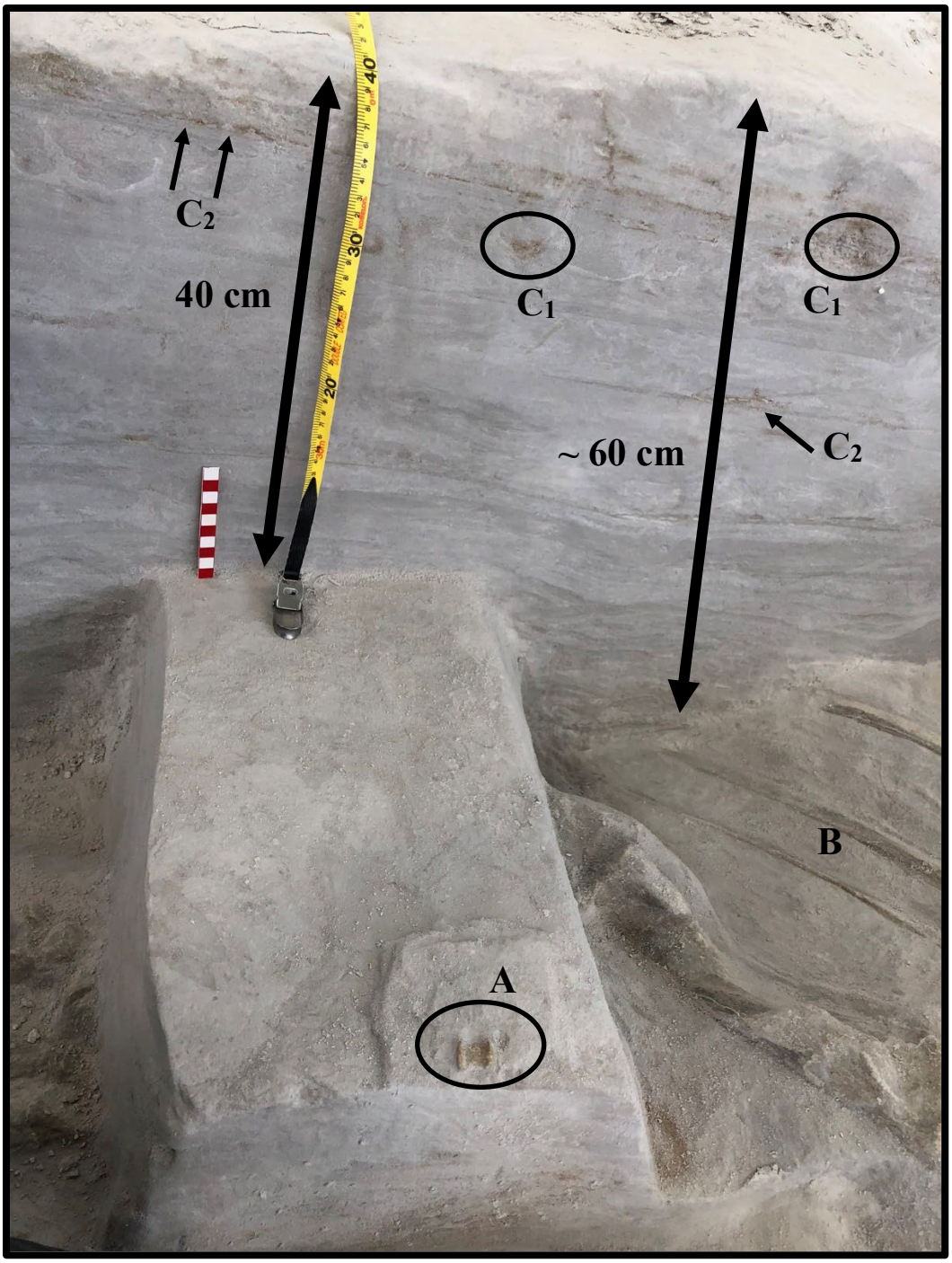

Figure 2. 5: At a shallower depth, approximately 30-40 cm from the surface is the location of the scattered bone, including a knuckle (A) and other smaller scattered remains. The location of the *in situ* intact rib cage is marked by (B). Along the cross-section of the ash bed, there are light brown pockets containing sand grains (C_1) and layers of sand (C_2).

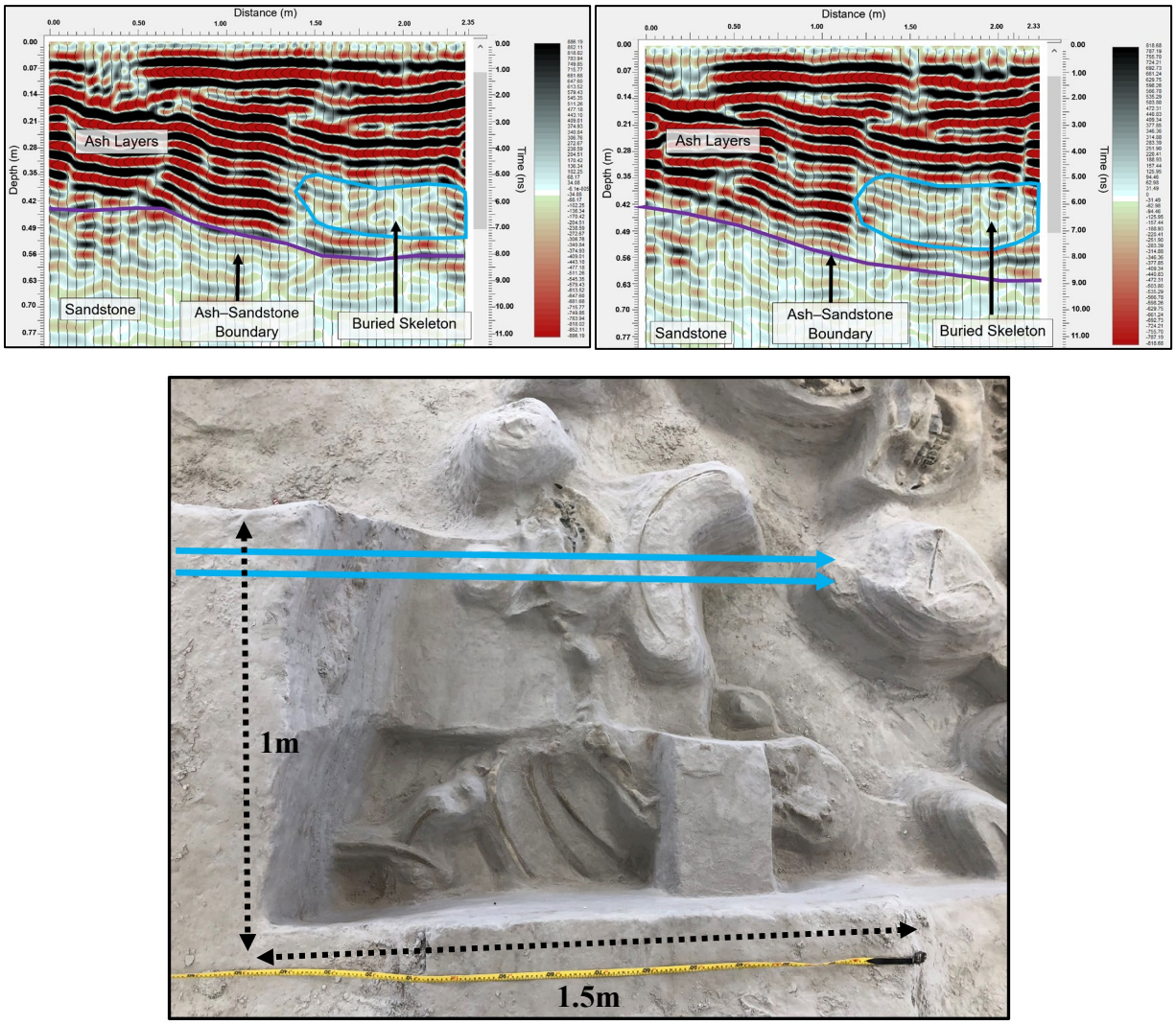

Figure 2. 6: Interpreted GPR lines 00 (top left) and 01 (top right). The location of "Rae's" rhino skeleton (blue circle) is characterized by low signal amplitude and reflector discontinuity when compared to the surrounding ash layers. The purple line marks the ash-sandstone contact (boundary). Below the purple line is the sandstone, which is a low amplitude region due to signal attenuation. The blue arrows in the photograph mark the location of the two GPR lines.

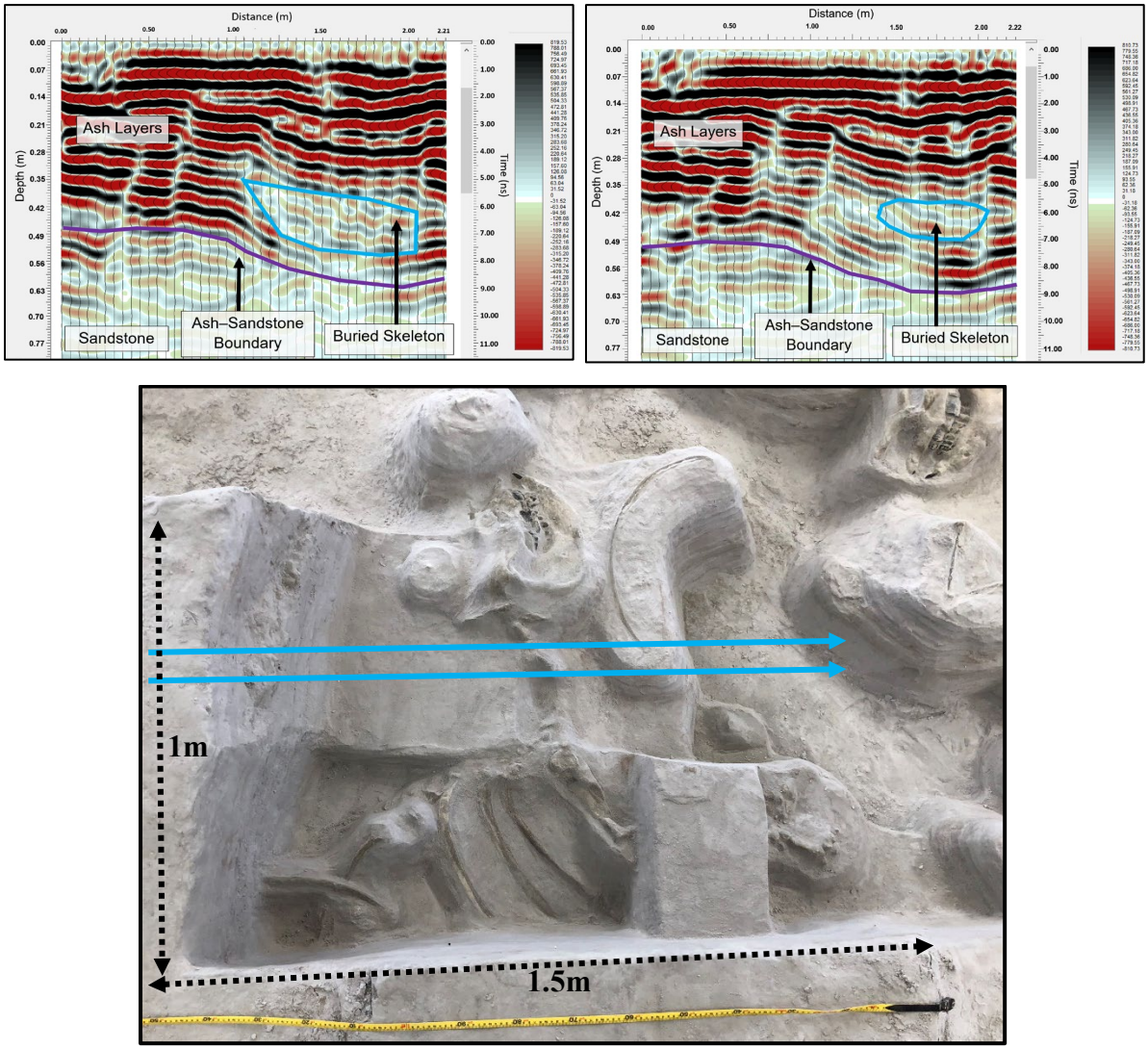

Figure 2. 7: Interpreted GPR lines 02 (top left) and 03 (top right marking the location of Rae's neck (light blue outline). The skeletal remains are characterized by low signal amplitude and discontinuous reflections. Below the purple line is the sandstone contact, which is a low-amplitude GPR region due to signal attenuation. The blue arrows in the photograph mark the locations of the two GPR lines.

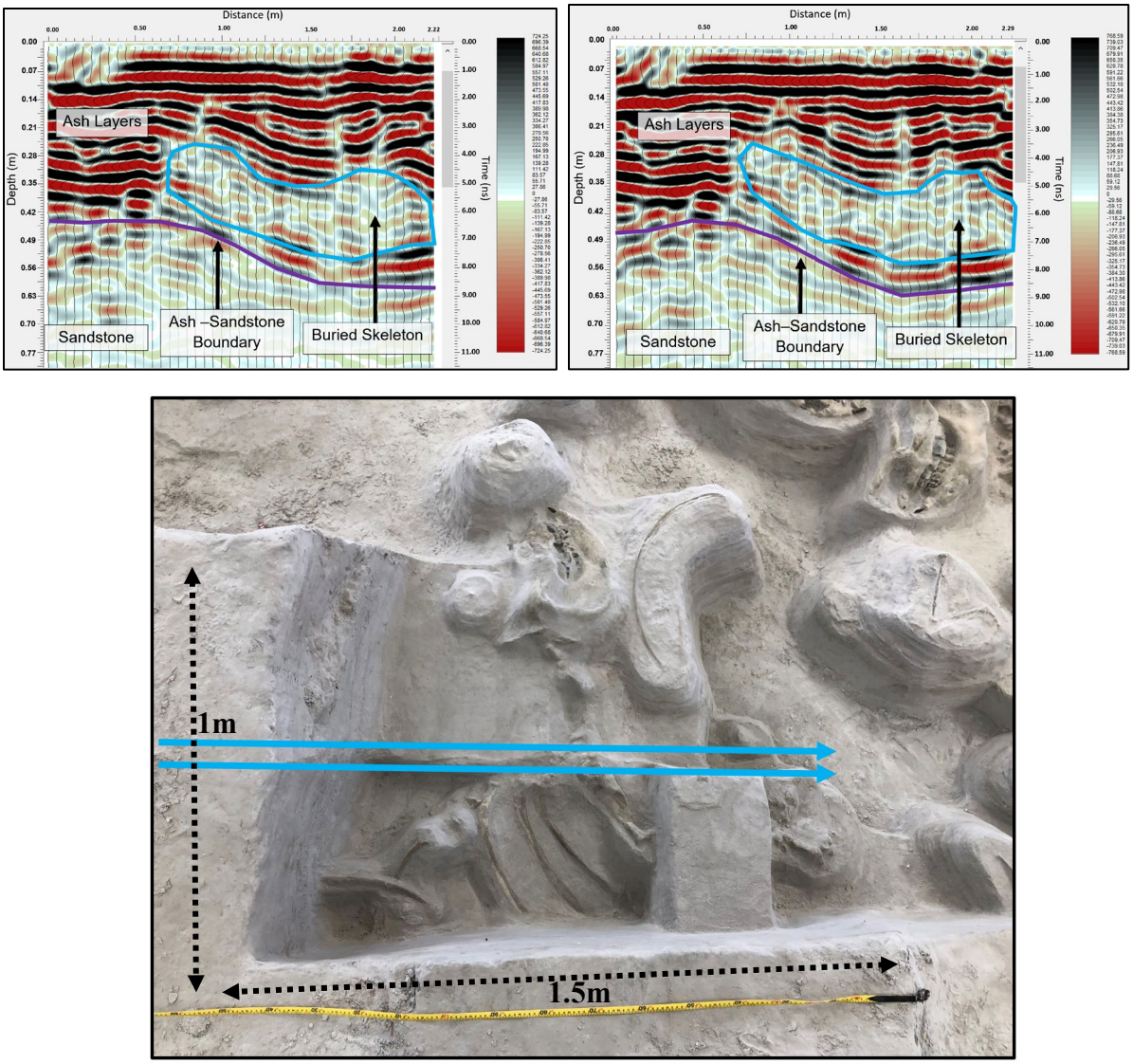

Figure 2. 8: Interpreted lines 06 (top left) and 07 (top right) taken over the center of the survey area, which is approximately the location of the neck and ribcage of the rhinoceros. Rae's location was detected by the loss of energy and discontinuous reflections (blue outline). The purple line marks the ash-sandstone contact (boundary). The blue arrows in the photograph mark the location and direction of the two GPR lines.

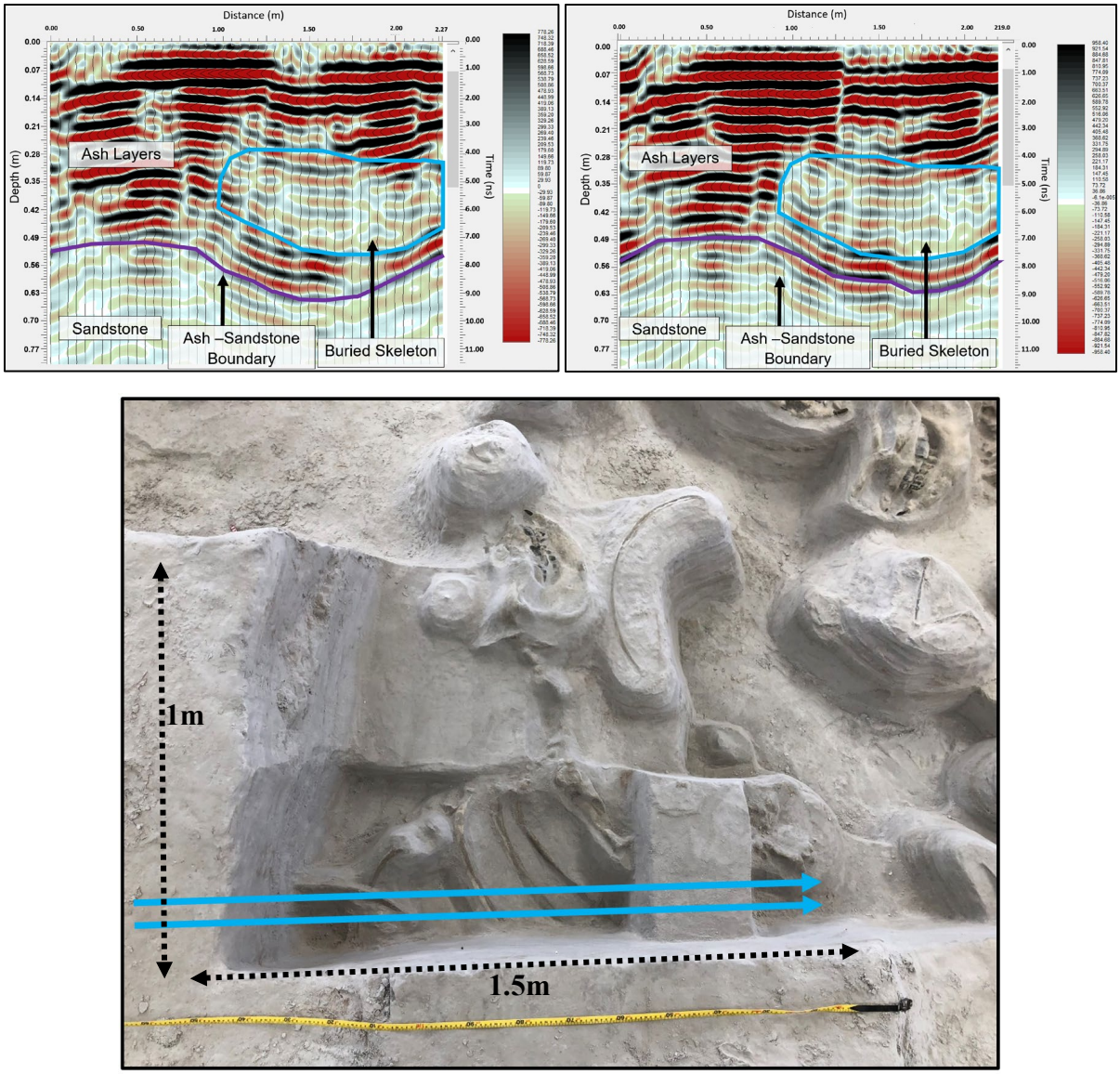

Figure 2. 9: Line 11 (top left) and line 12 (top right) are interpretated with the location of largest diameter of the skeletal remains. The blue arrows in the photograph indicate the location and direction of the two GPR lines. The purple line marks the ash-sandstone contact (boundary).

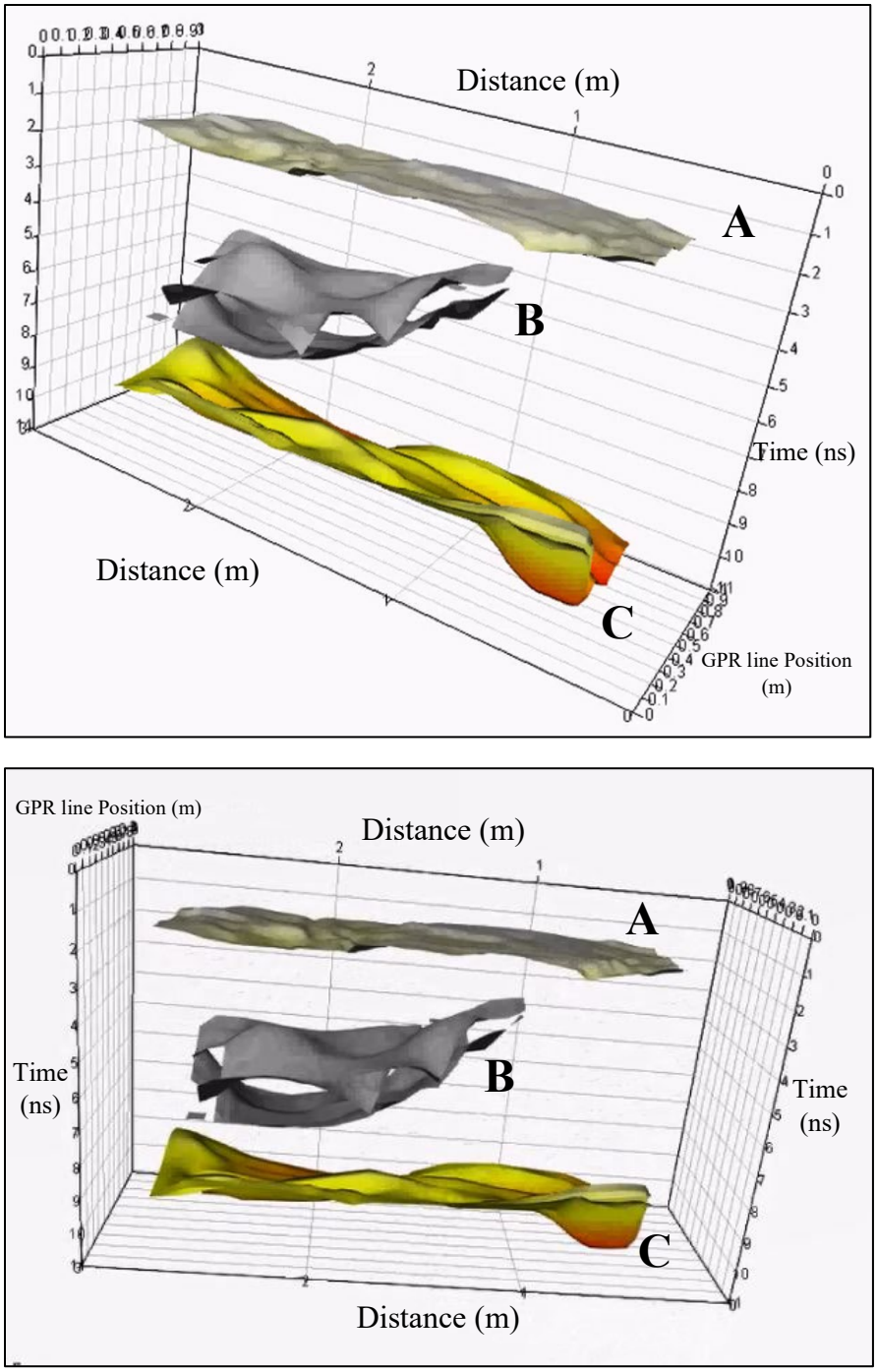

Figure 2. 10: Three-dimensional diagram of the GPR data showing the uppermost continuous ash layer (**A**), the top and bottom of Rae's skeleton delineated as the region of low-amplitude discontinuous reflections (**B**), and the ash-sandstone contact beneath the Rae's skeleton (**C**).

Chapter 3. GPR Imaging of Ash Beds and Tuffaceous Sandstone

3.1 Background

As noted in Chapter 1, a paleodepression that was once the site of an animal watering hole has been identified at Ashfall Fossil Beds. The depression favored the accumulation of large amounts of ash after the volcanic eruption. Tucker (2014) and Smith (2018a) recorded a sand and ash mixture in the lower portions of the ash bed within the Skeleton Zone, which is annotated in the stratigraphic column in Figures 1.6 and 1.7. Sand found within this region originated from the underlying sandstone unit comprising the paleodepression. Furthermore, some sand is present in the ash above the excavated rhinoceros (Figure 2.5). The occurrence of sand in the ash is likely a product of eolian deposition and contributions by sheetwash in the paleodepression.

The 1 GHz frequency GPR data presented in Chapter 2 show a distinct reduction in reflector amplitude at the contact between the volcanic ash and underlying sandstone (Figures 2.6-2.10). In the following section, I correspond the GPR response to the sandstone in the 1 GHz and 500 MHz frequency data and map the ash-sandstone contact across the entire survey area.

3.2 Determining Depth of Ash-Sandstone Contact Using GPR

To test the ability of the GPR to detect the ash-sandstone contact, two GPR lines were collected along an exposed section of ash deposits overlaying the sandstone (Figure 3.1). Each line was acquired using the 500 MHz and 1 GHz frequency antennas to examine the GPR response to the ash layers and sandstone contact. The GPR lines were acquired parallel to the exposed outcrop of ash and sandstone, and approximately 0.5 m from the outcrop face. Figure

3.1 shows the exposed section of ash and sandstone, with the boundary marked by a change in color and texture.

Figures 3.2 and 3.3 show the processed 1 GHz and 500 MHz frequency profiles along with the depths to the ash-sandstone contact. These depths were measured at four locations and ranged from 0.4 to 0.7 m. Both frequency profiles exhibit continuous, sub horizontal, strong reflections of ash layers. GPR signal amplitude strength degrades rapidly below the ash–sandstone contact. The two radar profiles image the same subsurface features in Figure 3.2 and Figure 3.3. As expected, the 1 GHz data exhibits higher resolution imaging but loses amplitude strength with depth. In comparison, the 500 MHz does not lose as much amplitude strength and can image deeper within the sandstone.

Figure 3. 1: Image of the 500 MHz frequency antenna deployed to test the depth to sandstone along the known sandstone contact (dashed line).

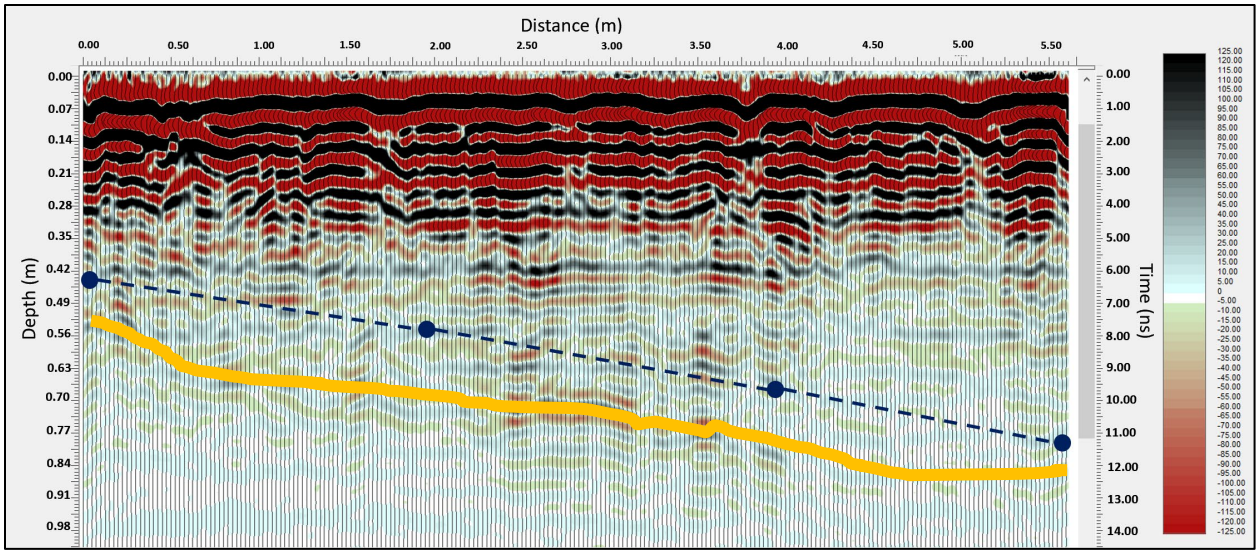

Figure 3. 2: Processed 1 GHz frequency GPR line along with measured depth to the ash-sandstone contact. The blue circles correspond to the locations of depth measurments made every 2 m along the exposed profile. The orange line is the GPR estimated ash-sandstone contact which appears deeper.

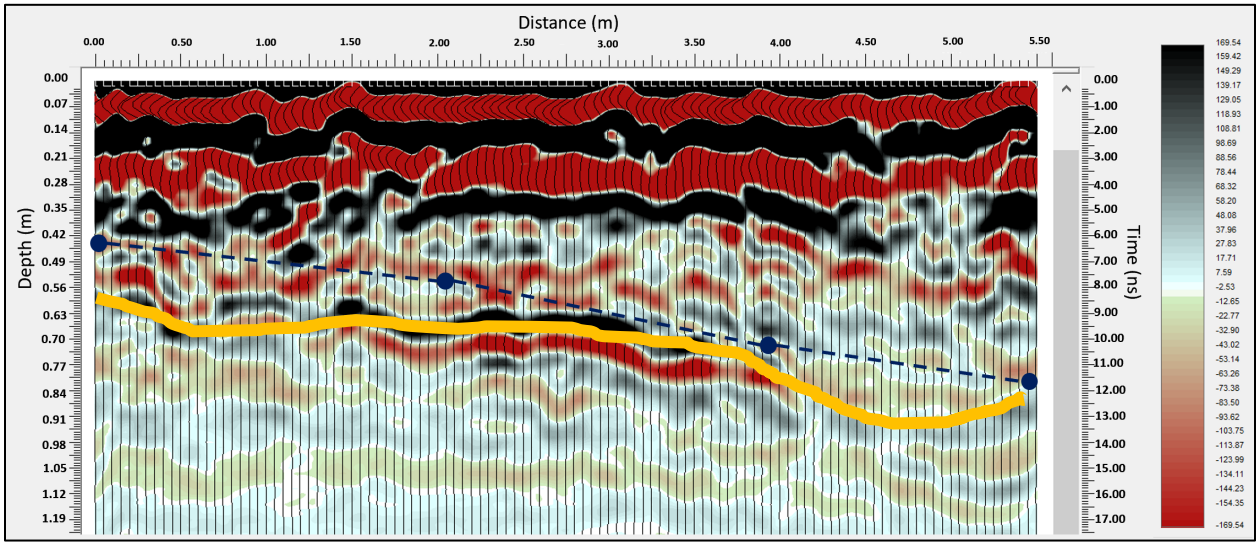

Figure 3. 3: Processed 500 GHz frequency GPR line along with measured depth to the ash-sandstone contact. The blue circles correspond to the locations of depth measurments made every 2 m along the exposed profile. The orange line is the GPR estimated ash-sandstone contact which appears deeper.

3.3 GPR Survey of the Ash-Sandstone Contact

The contact between the ash layers and underlying sandstone is seen in the GPR cross sections as a loss in amplitude, which is consistent with the previous investigation results. Throughout the site, the depth to the top of the sandstone varies, with the thickness of the ash bed progressively increasing towards the northwestern portion of the GPR survey. Overall, both the 1 GHz and 500 MHz datasets detected the ash-sandstone contact. By tracking the change in GPR signal amplitude, the top of the sandstone was traced across the study area (see Figure 3.4 as an example).

In Figures 3.2, the 1 GHz data image shows initial signal attenuation at shallower depths than the 500 MHz data (Figure 3.3). To estimate how accurately the GPR images the ash-sandstone contact, a percent error was calculated (equation 4) using the measured sandstone depths from the surface to the interpreted depths from the GPR images seen in Figures 3.2 and 3.3. Table 3.1 and 3.2 lists the measured depths and interpreted depths for each frequency. Overall, the percent error revealed a higher error range (20.4%) for the 1 GHz data as compared to the 500 MHz error (17.8%). It's also noted that the accuracy of both datasets improves as the ash-sandstone contact increases in depth – particularly for the 500 MHz frequency data.

$$(4)\ \text{Percent error} = \left|\frac{measured\ value - real\ value}{measured\ value}\right| \times 100\%$$

1 GHz Sandstone Contact Measurements					
Distance (m)	**Actual (m)**	**Measured (m)**	**Relative error**	**Individual Percent error**	**Average of total percent error**
0	0.43	0.56	0.302326	30.23256	20.3796%
2	0.50	0.66	0.32	32	
4	0.70	0.80	0.142857	11.42857	
6	0.80	0.84	0.05	5	

Table 3. 1: Measured values of the actual sandstone contact to the GPR interpretation of the ash-sandstone contact. Relative error is the subtraction of the measured by the actual measured depths divided by the actual measured depth to sandstone. The percent error was then found by multiplying by 100 percent. Over the entire surveyed line the deduced average percent error across the test line was 20.4%.

500 MHz Sandstone Contact Measurements					
Distance (m)	**Actual (m)**	**Measured (m)**	**Relative error**	**Individual Percent error**	**Average of total percent error**
0	0.43	0.59	0.372093	37.2093	17.8023%
2	0.50	0.67	0.34	34	
4	0.70	0.70	0	0	
6	0.80	0.80	0	0	

Table 3. 2: Measured values of the actual sandstone contact to the GPR interpretation of the ash-sandstone contact. Relative error is the subtraction of the measured by the actual measured depths divided by the actual measured depth to sandstone. The percent error was then found by multiplying by 100 percent. Over the entire surveyed line the deduced average percent error across the test line was 17.8%.

(A)

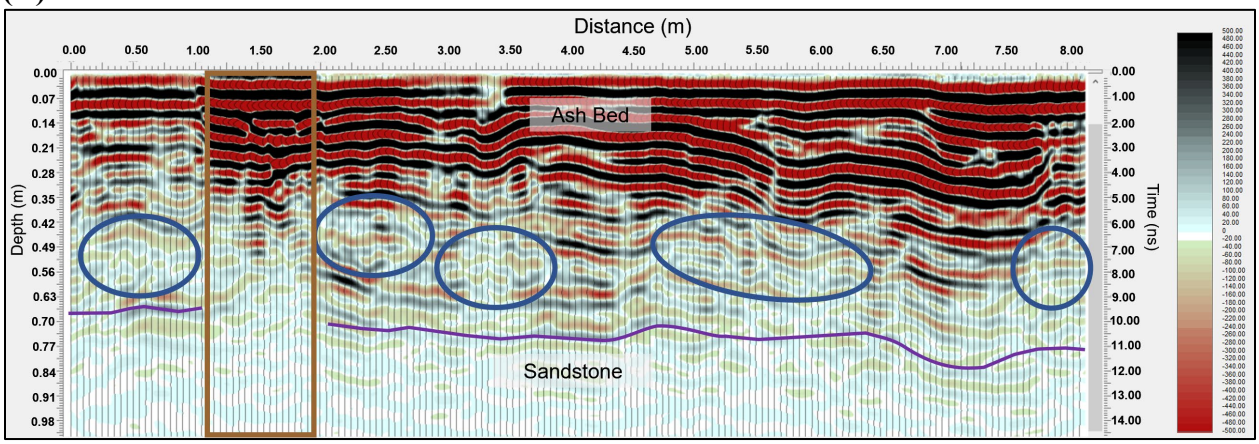

(B)

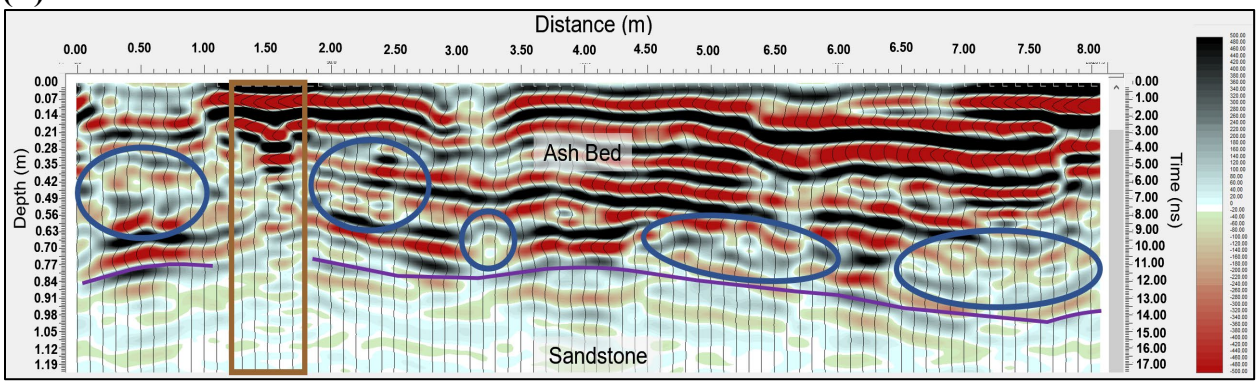

Figure 3. 4: Processed GPR profiles of the unexcavated quadrants within the Hubbard Rhino Barn. (**A**) 1 GHz frequency data, and (**B**) 500 MHz frequency data. The purple line represents the ash-sandstone contact. The brown boxed region is the location of a void (trench). Interpreted animal remains are identified by discontinuous, lower amplitude reflections in both sections and are circled in blue.

3.4 Discussion

In Chapter 3, the goal is to interpret the location of the ash-sandstone contact within each quadrant and to identify the accuracy of our measurements. The GPR survey conducted in an excavated area of the site where the ash-sandstone contact is visible validated that the ash-sandstone contact is indicated by a reduction of radar signal amplitude. The reduction of radar signal is attributed to the higher electrical conductivity of the underlying sandstone. After identifying the ash-sandstone contact, the 1 GHz and 500 MHz datasets were used to map the thickness of ash deposits (or the depth to the top of the sandstone) across the unexcavated section of the Hubbard Barn (Figure 3.5 and 3.6). In the 500 MHz frequency data, the depth of the ash-sandstone contact is estimated to range from 0.8 m to 1.5 m. This is deeper than the 1 GHz data interpretation which ranges from 0.6 m to 1.0 m across the site. Based on the results of this chapter, it is estimated that the accuracy to the depth of the ash-sandstone contact is most likely 0.8 m to 1.5 m because the 500 MHz had a lower percent error overall at estimating these depths.

Furthermore, interpretation of the GPR 1 GHz and 500 MHz grids tracing the ash-sandstone contact (Figure 3.5 and 3.6) shows that the thickness of the ash beds increases with distance as we move further from the excavated area of the Barn. The 1 GHz frequency data indicates that the ash bed is about 0.60 to 0.90 m thick in Quadrant O, and 0.80 to 1.20 m thick in Quadrant M. In addition, in the northern portion of the GPR survey in quadrant M, an anomalous area is shown that suggests greater depth to the sandstone. This increase in measured ash thickness is likely due to the higher elevation of the subsurface topography at the location of the site.

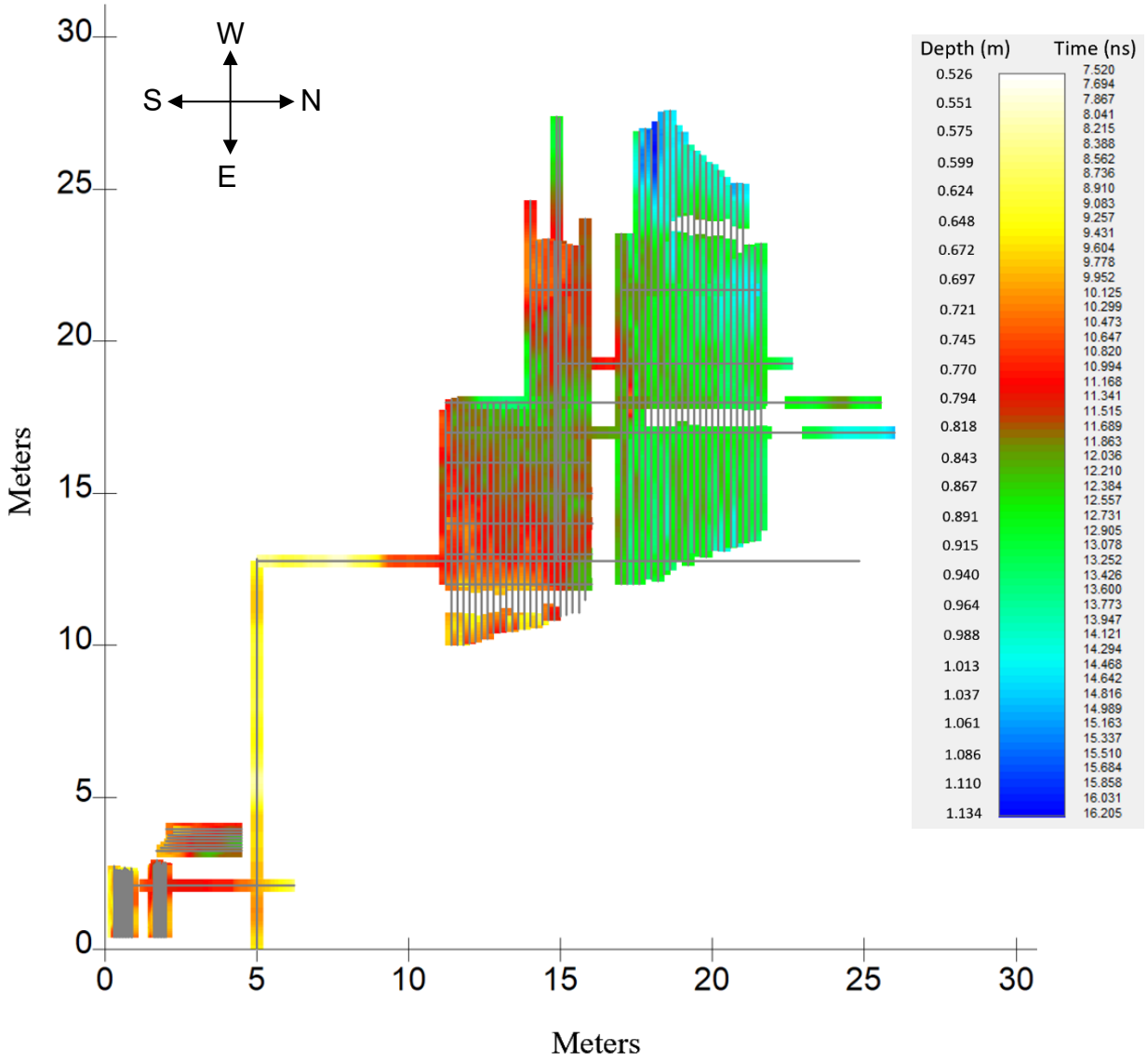

Figure 3.5: GPR map of the ash thickness (or depth to sandstone from surface) using the 1 GHz data at the Hubbard Barn in Ashfall Fossil Beds. The thickness of the ash ranges from 0.6 to 1.0 m.

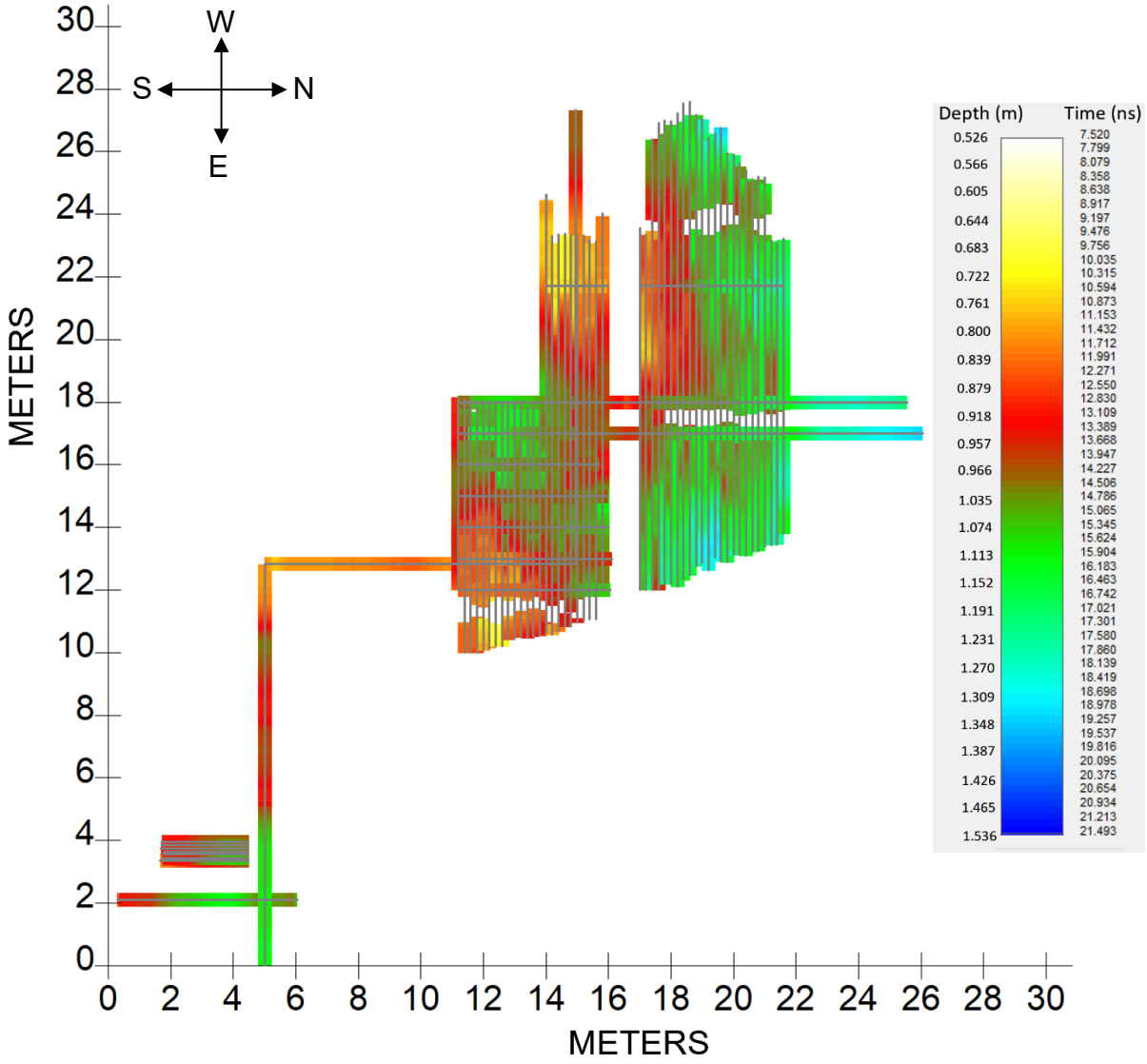

Figure 3.6: GPR map of the ash thickness (or depth to sandstone from the surface) using 500 MHz data at the Hubbard Barn in Ashfall Fossil Beds. Depths range from 0.6 m to 1.3 m as the survey moves north.

Chapter 4. GPR Imaging of Ichnofossils

4.1 Identification of a Known Animal Burrow

Fossil animal burrows filled with ash and sand have been identified at Ashfall Fossil Beds (Tucker et al, 2014; Smith et al., 2018b), with most occurring in the Skeletal Zone and lower parts of the Dead Zone (refer to Chapter 1.2.2). The burrows tend to have an elliptical shape (Figure 4.1) and are 25-75 cm in diameter. Some burrows extend to a depth of 75 cm below the top of the ash bed, and bone fragments have been recorded in many burrows (Tucker et al., 2014). In addition, the walls of burrows are often cemented with calcium carbonate along with animal claw marks (John Smith, personal communication, 2021). Tucker et al. (2014) suggested that the burrows are products of scavenging carnivores that dug into the ash in search of food soon after the volcanic eruption. After time, these burrows are infilled with mixtures of sand and ash, while other burrows contain some mixture of sand. In some cases, these animal burrows can be exhumed partially by other smaller animals searching for carcass remains under the ash. Furthermore, it is common that smaller burrows are found within larger burrows resulting in different infill compositions.

An intact, large elliptical animal burrow was identified within the GPR survey area of the investigation (Figure 4.2). Viewed from above, it is apparent that the large burrow is filled with two separate concentrations of sediment: one consisting mostly of sand and the other consisting of volcanic ash (Figure 4.3A). After close inspection, a smaller darker colored burrow can be found within the larger animal burrow. The sand-filled burrow is within the larger ash-filled burrow which most likely penetrated the sandstone unit. The major and minor axis of the entire elliptical burrow is 70 cm and 35 cm long, respectively (Figure 4.3B).

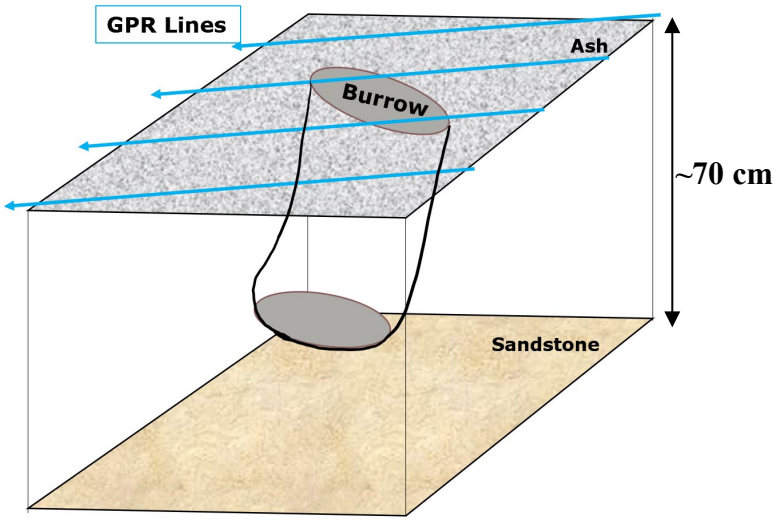

Figure 4. 1: Diagram of a typical fossil animal burrow at Ashfall Fossil Beds (image design from personal communications with Smith 2021).

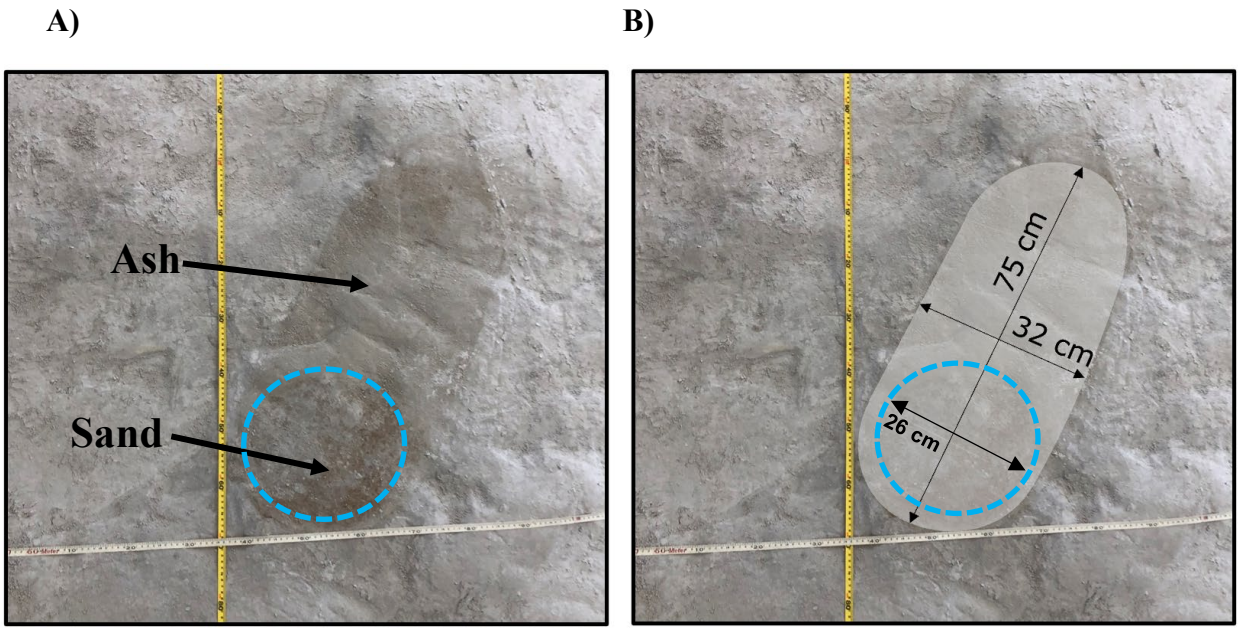

Figure 4. 2: A-B: Plan-view photograph of the two intact animal burrows imaged by GPR (shown in Figure 4.2). (**A**) Circled in blue is the smaller sand filled burrow located in lower portion of the larger elliptical burrow. The larger, elliptical burrow can be seen in a darker shade of grey in the ash bed. This can be suspected the larger animal burrow is comprised mainly of ash than sand. (**B**) Plan-view photograph showing the dimensions of the burrows.

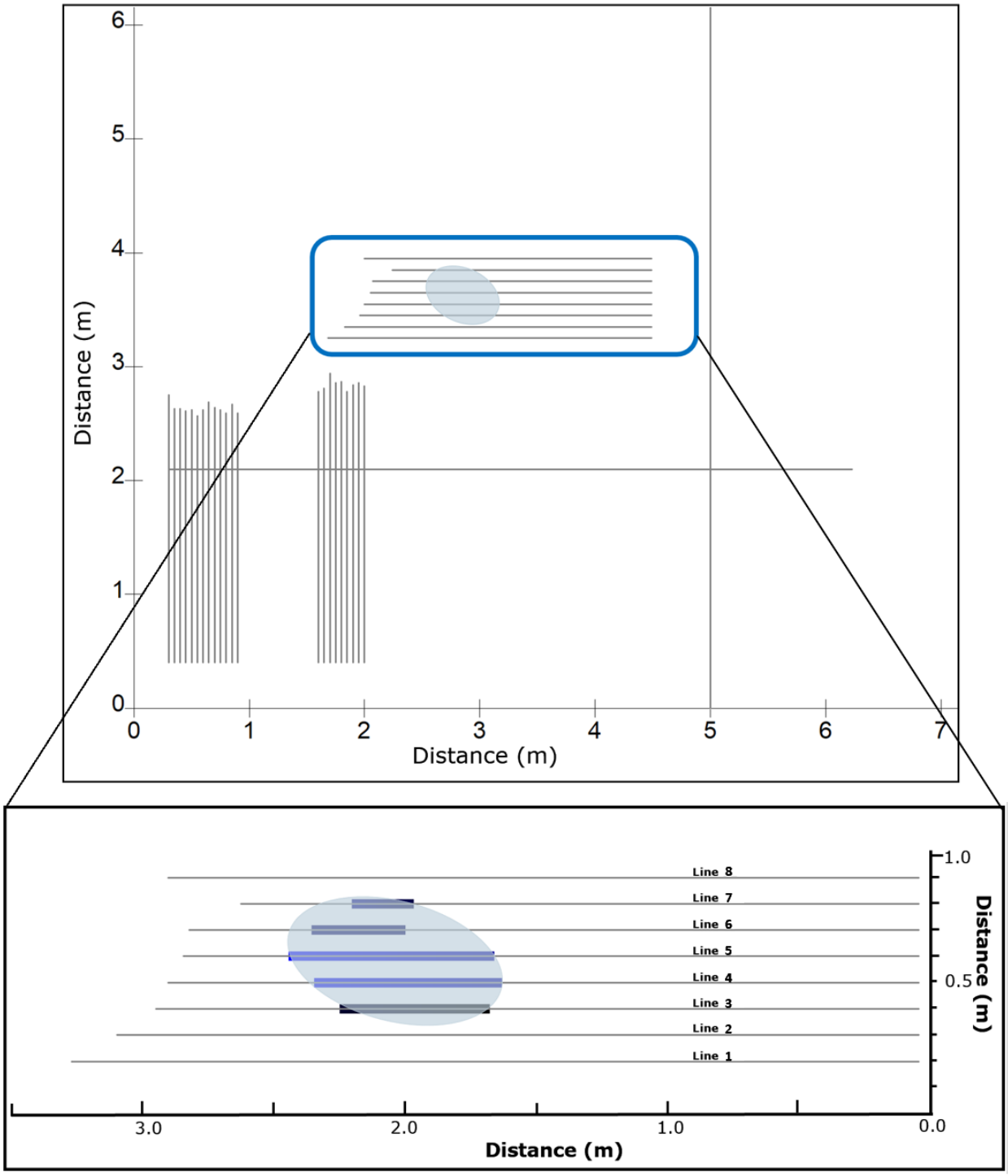

Figure 4. 3: Location map of large animal burrow (highlighted in blue) identified within the GPR survey area. The zoomed-in map shows the location of GPR lines and the surface expression of the burrow intersected by the radar profiles. This survey located in the southwest section of the Hubbard Barn (see Figure 1.12).

4.2 GPR Imaging of a Fossil Animal Burrow

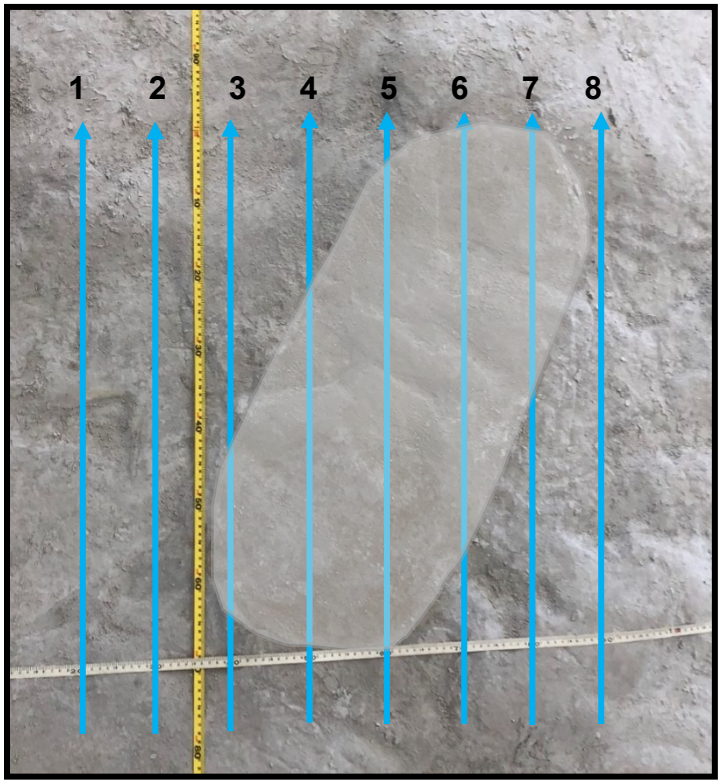

Figure 4.4: GPR survey lines labeled 3 through 7 traverse the top of the burrow shown in Figures 4.2 and 4.3.

Eight GPR lines were acquired with the 1 GHz and 500 MHz antennas with 0.1 m line spacing over the animal burrow shown in Figures 4.3 and Figure 4.4. During the acquisition of the GPR data, the area of the burrow was noted along the survey lines. The data were processed as described in Chapter 1. The GPR lines and profiles are shown in Figures 4.4 and 4.8 and uninterpreted lines can be found in Appendix A5 to A8. The location of the edges of the animal burrow along the GPR profiles are marked by inverted blue triangles in Figures 4.5 to 4.8.

Lines 4 and 5 (Figure 4.3) intersect at the largest dimensions of the animal burrow. The shallowest reflectors (upper two reflections 0-4 ns time) exhibit small downward bending under the blue triangles marking the location of the burrow (Figures 4.5-4.8). Bending of the

uppermost reflectors is evidence of changing radar wave velocity from the region outside the blue triangles (faster in the ash deposits) to the region between the blue triangles (slower in the deposits of mixed ash and silty sand). Lower velocity within the burrow material results in longer travel time compared to the ash layers outside the burrow, which appears as a downward bending of the shallow burrow reflectors. Deeper in the GPR profile (4 – 9 ns time), between the blue triangles and outlined by a yellow box in Figures 4.5-4.8, reflectors are low amplitude and discontinuous, which is consistent with the presence of animal bone (see Chapter 2). Similar discontinuous, low-amplitude reflectors in the deeper Skeleton Zone (4 – 9 ns time) occur in lines 3 to 7, suggesting the presence of skeletal remains near the base of the animal burrow. Discontinuous, low-amplitude reflector anomalies also occur outside the boundaries of the burrow observed at the surface; hence, the carcass scavenged by the burrowing animal may extend beyond the surface expression of the burrow.

4.3 Interpretation of Animal Burrow

This chapter evaluated the GPR response over a large animal burrow, which is a common ichnofossil seen within the Hubbard Barn. The animal burrows have different dielectric properties than the surrounding ash due to a different sediment composition, typically a mix of ash and silty sand, and overall stratigraphic disruption compared to the undisturbed ash layers. GPR profiles imaged across the large animal burrow suggest that the biogenic feature has a shallow, stratified interior similar to adjacent ash layers but with deeper disturbed sediment (Figure 4.5 to Figure 4.8). The vertical edges of the burrow reveal a velocity change within the 1 GHz data noted by the orange arrows (Figure 4.5 C – D and Figure 4.6 A-C). Within the highlighted region of Figure 4.7 C-D and Figure 4.8 A-C, the 500 MHz data shows larger

discontinuous reflections and visible loss of amplitude strength over the animal burrow. Overall, in both frequencies, GPR lines intersecting the animal burrow show reflector discontinuities aligning with the lateral extent of the animal burrow. In addition, both frequencies show that the deeper profile of the burrow exhibits noticeable discontinuous, low-amplitude reflectors that suggest the presence of skeletal remains. Future excavation of the burrow will provide an opportunity to verify the observations made in the GPR profiles.

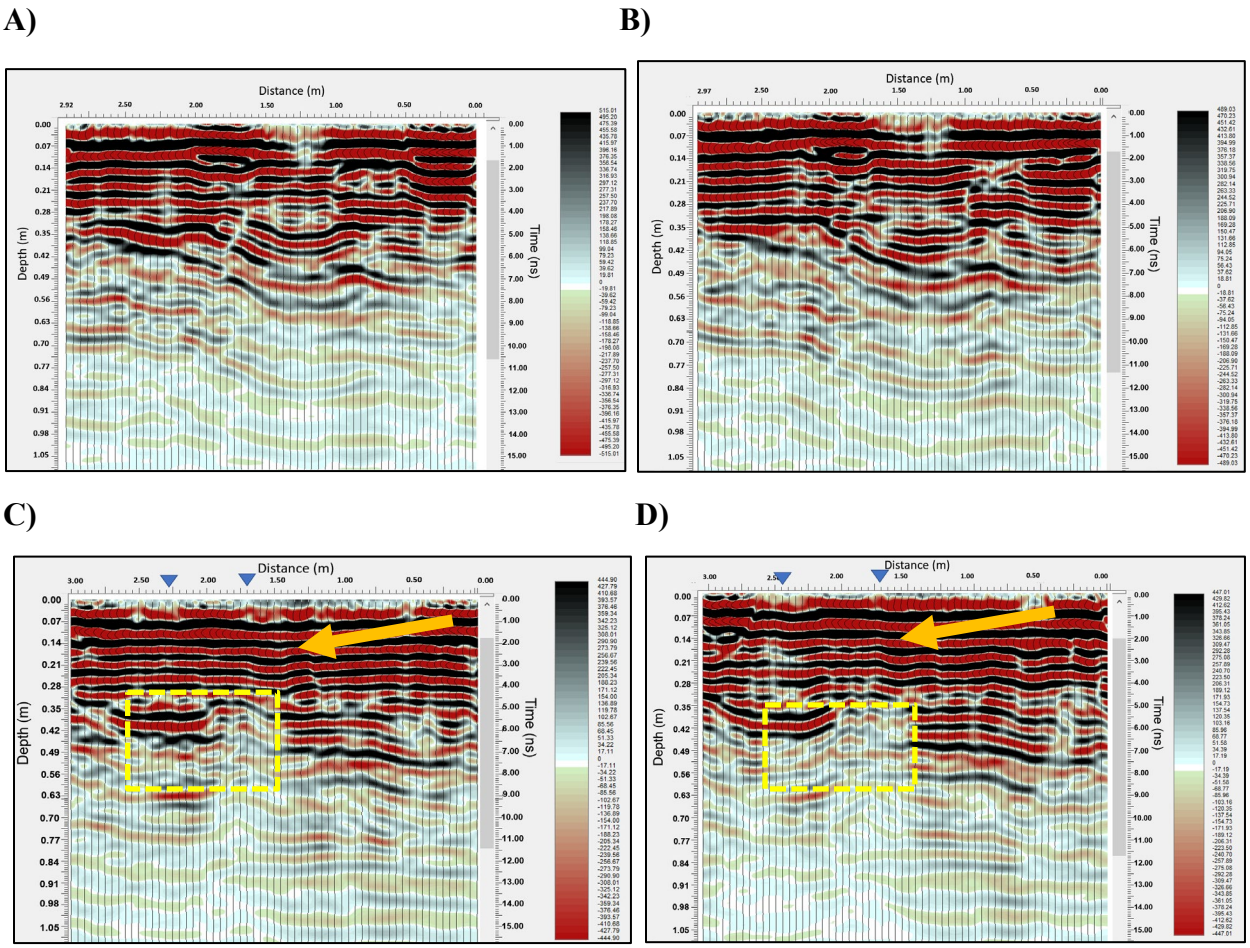

Figure 4.5: (A) Line 1 (A) and line 2 (B) are 1 GHz frequency GPR profiles over the surface expression of the animal burrow. Line 3 (C) and line 4 (D) intersect the burrow on the surface at the locations marked by the blue triangles. The orange arrow identifies disruptions beneath intersecting animal burrow. The yellow boxes represent low amplitude and discontinuous reflectors below the blue triangles.

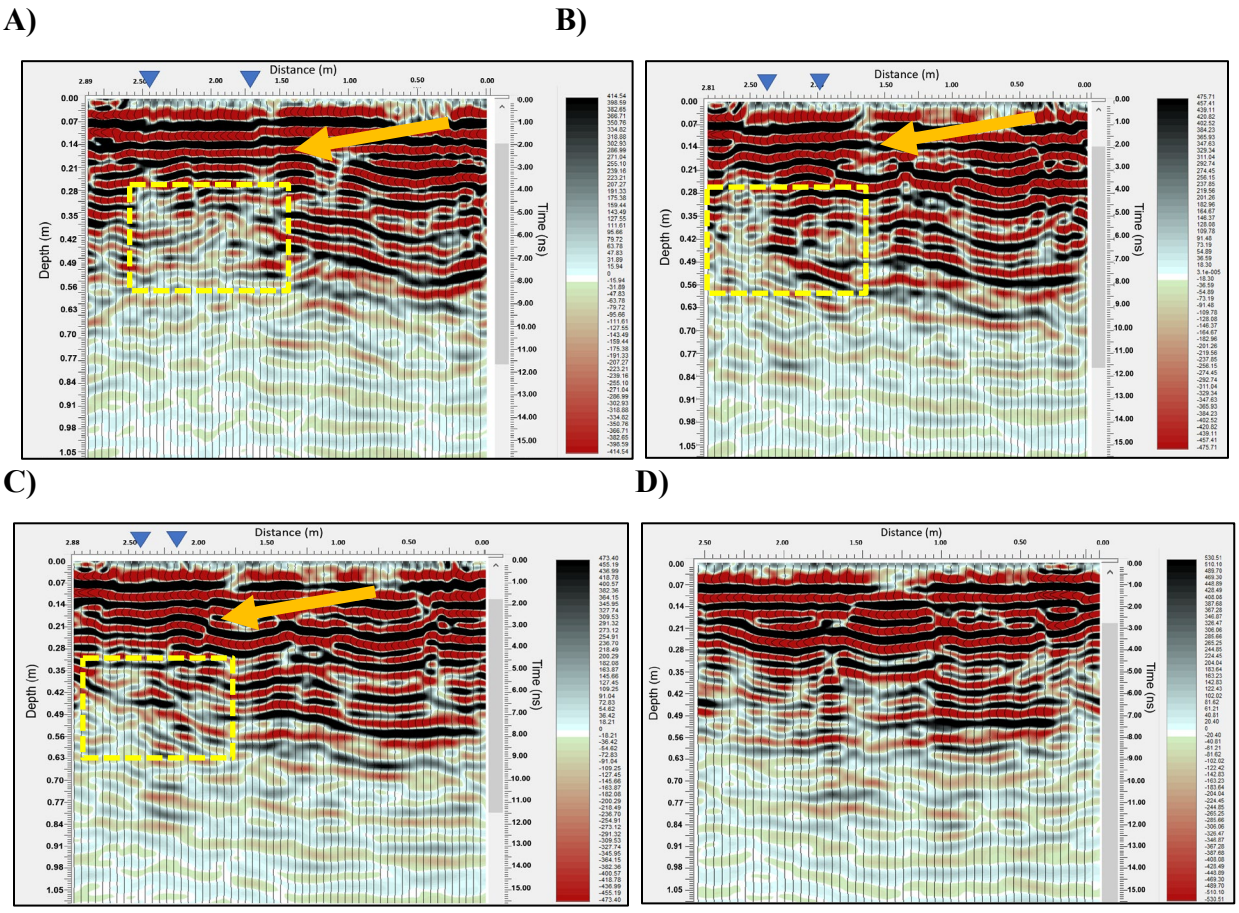

Figure 4.6: Annotated 1 GHz frequency GPR lines 5-8 (A-C) indicating the location a burrow between the blue triangles. Line 8 (D) does not intersect the burrow on the surface by the GPR. The orange arrow identifies disruptions beneath intersecting animal burrow. The yellow boxes represent low amplitude and discontinuous reflectors below the blue triangles.

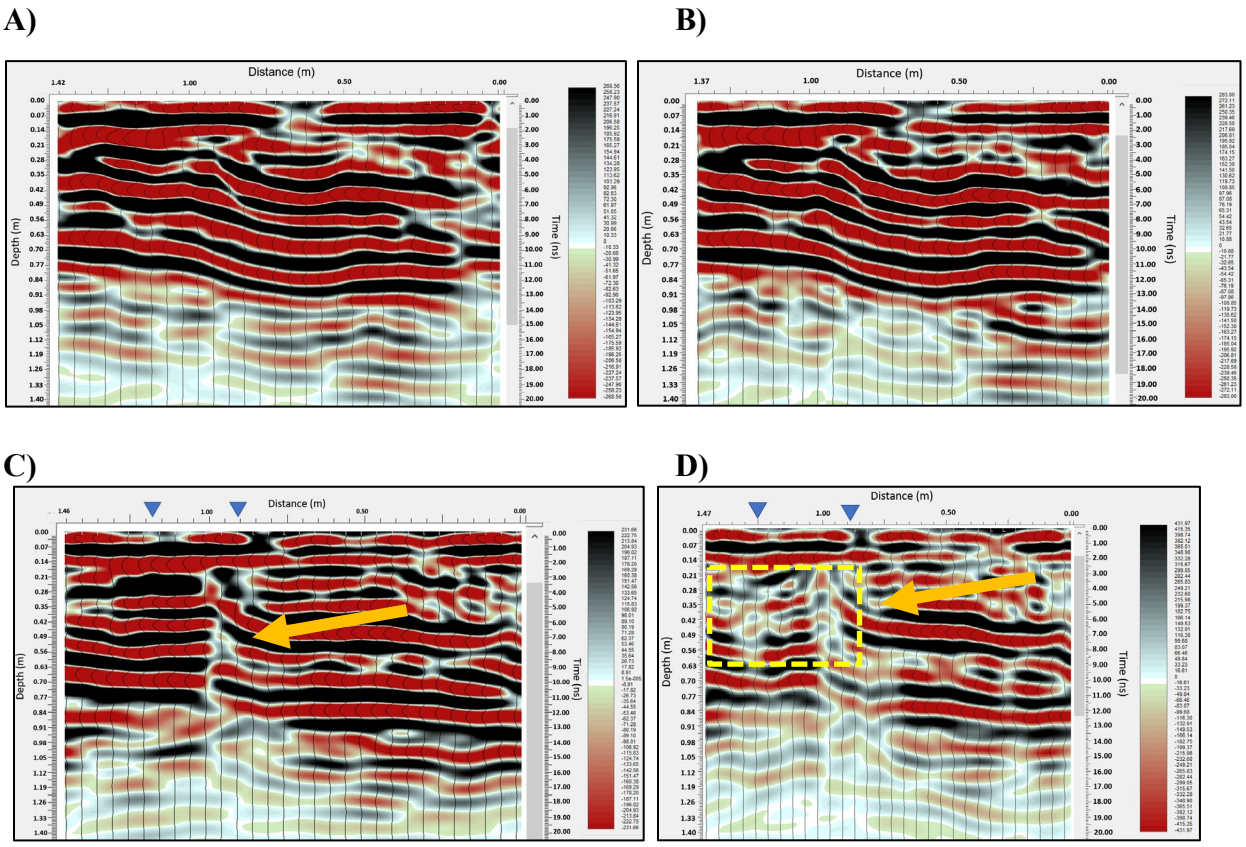

Figure 4.7: Line 1 (A) and line 2 (B) are 500 MHz frequency GPR profiles over the surface expression of the animal burrow. Line 3 (C) and line 4 (D) intersect the burrow at the locations marked by the blue triangles. The orange arrow identifies disruptions beneath intersecting animal burrow. The yellow boxes represent low amplitude and discontinuous reflectors below the blue triangles.

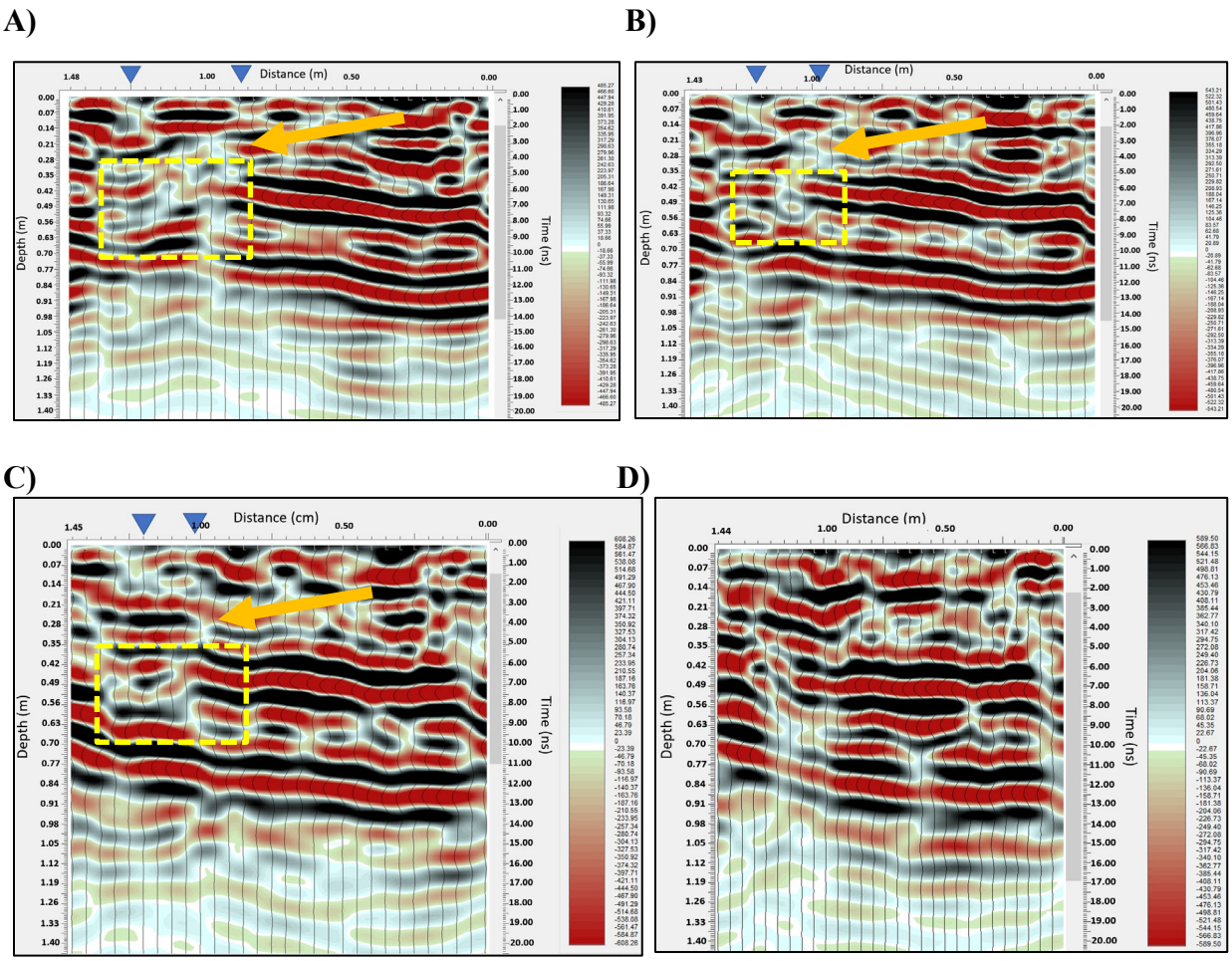

Figure 4.8: Annotated 500 MHz frequency GPR lines 5-8 (A-C) indicating the location a burrow between the blue triangles and circled area is the suspected profile of the animal burrow. Line 8 (D) does not cross over the burrow. The orange arrow identifies disruptions beneath intersecting animal burrow. The yellow boxes represent low amplitude and discontinuous reflectors below the blue triangles.

Chapter 5: Interpretation of the GPR Characteristic Features

Chapters 2, 3, and 4 tested distinct locations of the study site to show the effectiveness of GPR for imaging ash layers, buried prehistoric animal remains, animal burrows, and the interface between ash deposits and the underlying sandstone. In this chapter, I identify unique characteristics of these GPR anomalies to map the location of paleontological features over the entire unexcavated part of the Hubbard Barn at Ashfall Fossil Beds. Based on the results described in the previous chapters, four distinctive GPR anomaly characteristics are identified. These characteristics represent the suspected remains of buried skeletons, scattered bones, ichnofossils, and/or a combination of fauna and ichnofossils. The four distinct characteristics prevalent throughout the GPR survey data are classified as follows:

1. First characteristic: Limited extent (less than 1 m) with high loss of signal amplitude and discontinuous reflections. These signatures are surrounded by strong, continuous ash reflections and are located almost exclusively in the Skeleton Zone, which is within the lower section of the ash deposits, approximately 5-30 cm above the ash-sandstone contact. This section of the ash deposits is consistent with the location where fossilized animal remains excavated at the site have been identified (Figure 5.1A). These signatures are interpreted as isolated and intact skeletons.
2. Second characteristic: Expansive regions (greater than 1 m) with high loss of signal amplitude and discontinuous reflections. The second characteristic regions are the same as the GPR amplitude signatures seen in characteristic #1, but they have greater lateral extent (Figure 5.1B, 5.4B). This second GPR signature (Fig. 5.1B) is also located in the Skeleton Zone and extends vertically approximately 30 cm or more. This second characteristic is interpreted to be an assemblage of fauna. An assemblage of fauna is defined as multiple fossilized skeletal remains that lay close to one another.

3. Third characteristic: Locations with little to no loss of amplitude strength but with discontinuous reflections (Figure 5.2A). These GPR characteristics are found in the middle to upper section of the radar profiles, which corresponds with the Dead Zone. The third characteristic extends vertically approximately 20 cm and less than or equal to 1 m in the horizontal direction. Because these characteristics are located higher in the stratigraphic section, they are interpreted to be the location of ichnofossils or sheetwash.
4. Fourth characteristic: The fourth characteristic also exhibits little to no loss of amplitude strength and discontinuous reflections in the Dead Zone. However, these anomalies extend over a larger horizontal direction (> 1 m) (Figure 5.2B). Because of their stratigraphic position and size, these are interpreted as extensive ichnofossils, such as deposits of large horizontal rhizoliths, vertebrate animal tracks, and/or ant nests (refer to Chapter 1, section 1.2.2.1).

Figure 5.3 shows an interpreted representation of the first characteristic, the ash-sandstone contact, and an area of undisrupted ash that was tracked across the site. Three shallow, undisrupted ash layers were tracked in the Dead Zone. Because those ash layers were continuous across the site, any discontinuous reflections in them are interpreted to have occurred after deposition of the volcanic ash layers. This finding supports the interpretation that characteristics 3 and 4 are ichnofossils that developed after the deposition of the ash. This is different than the first two characteristics of skeletal remains, which were deposited at the same time as the deposition of the volcanic ash layers.

In Figure 5.4, maps of each of the individual characteristics can be seen across the entire GPR survey area of the Hubbard Barn. The mapped regions are conservative interpretations

(i.e., my most confident interpreted examples) of each characteristic found within the GPR survey area. Furthermore, Figure 5.4A shows the first characteristic anomaly found within the barn and is scattered across the quadrants. Unlike Figure 5.4A, Figure 5.4B represents the second characteristic that is predominant across the site. This characteristic is found densely spaced across the site, which supports the interpretation that these are mass bone assemblages. The third (Figure 5.4C) and fourth (Figure 5.4D) characteristics are primarily located within Quadrants O and M, which is consistent with current excavation results. However, this doesn't mean that the ichnofossils were not present in Quadrant Q. For example, the animal burrow described in Chapter 4 was located in Quadrant Q. More overburden (i.e. Dead Zone) has been removed from Quadrant Q to get closer to skeletal remains found in the Skeleton Zone.

(A)

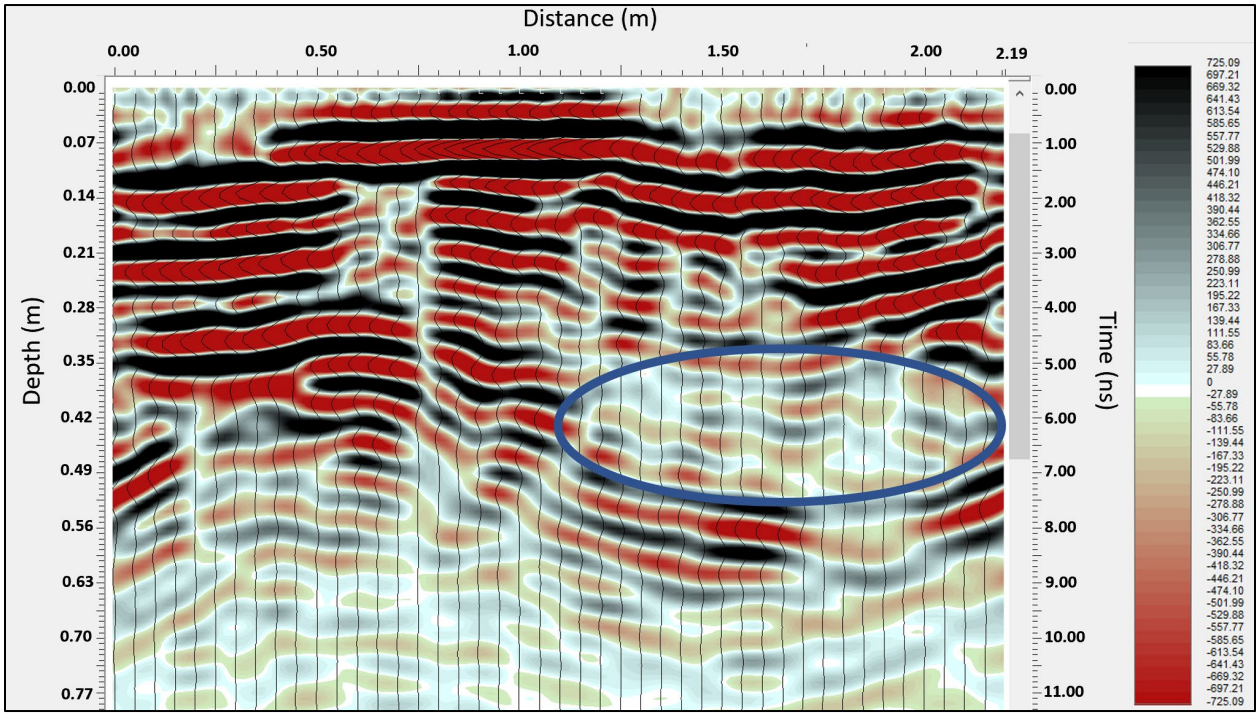

(B)

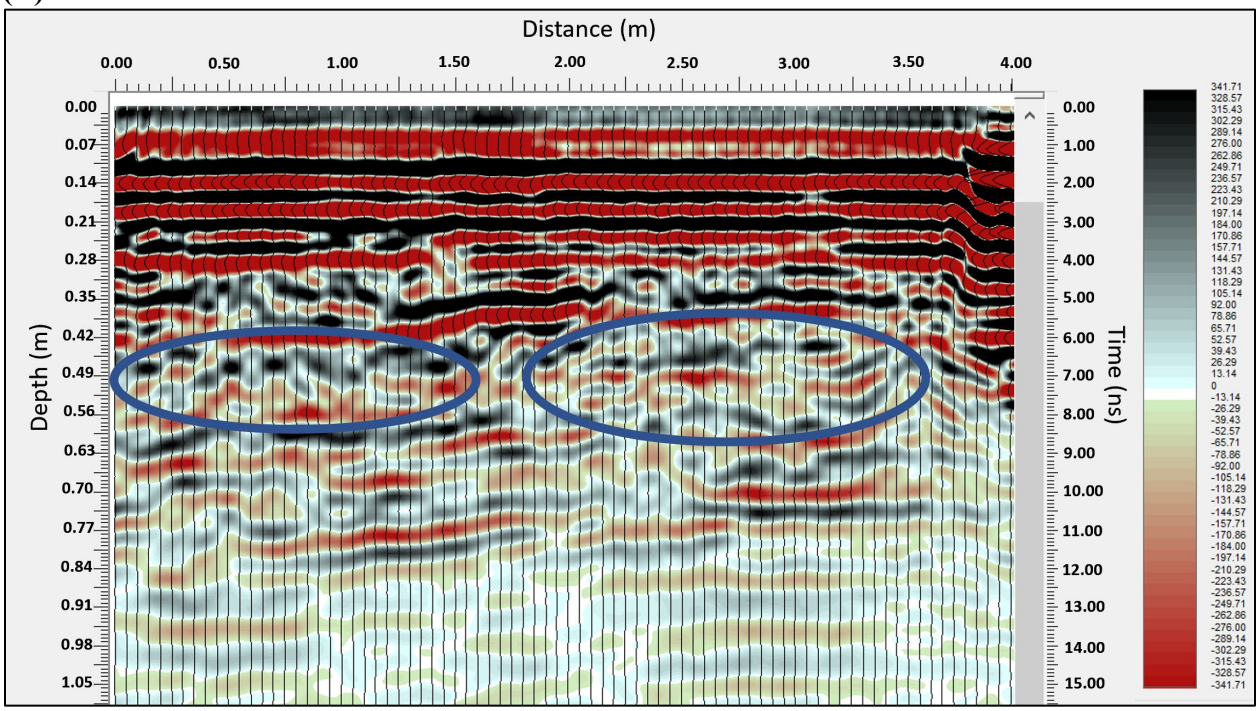

Figure 5. 1: Representative 1 GHz frequency GPR cross sections. The blue circles highlight the anomalies associated with the first characteristic (A) and second characteristic (B). (A) represents singular skeletons and (B) represents possible assemblages of skeletons.

(A)

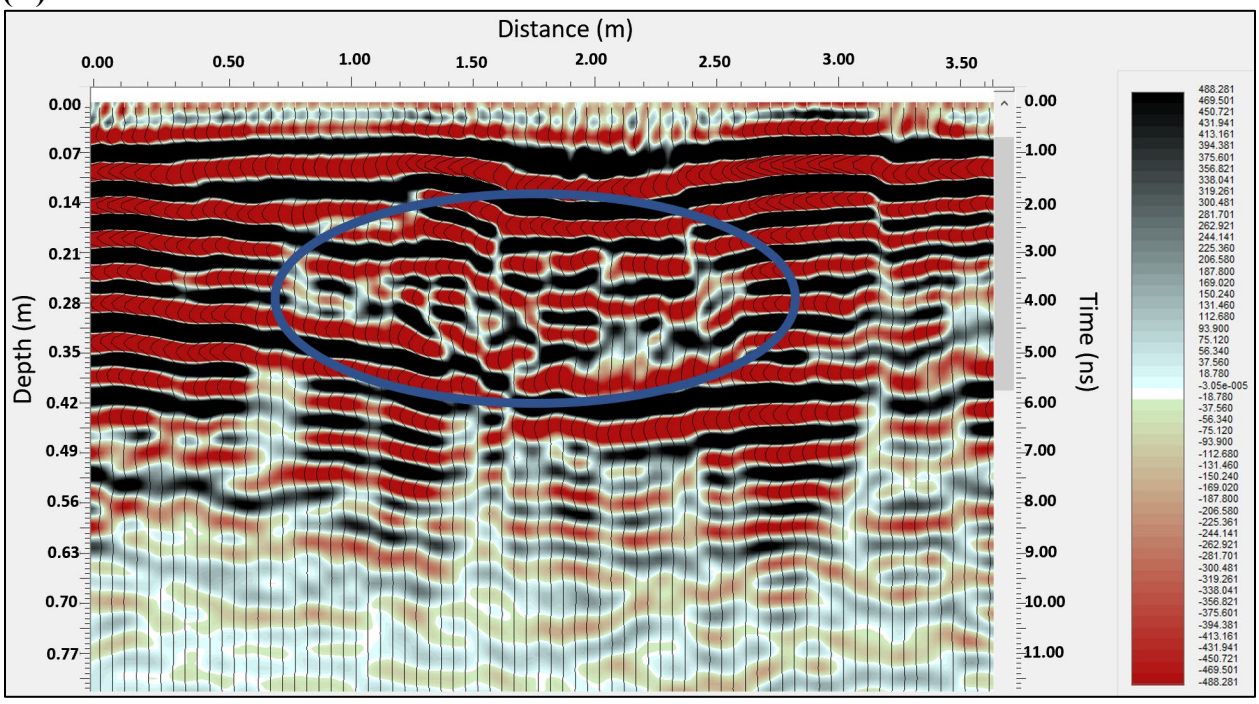

(B)

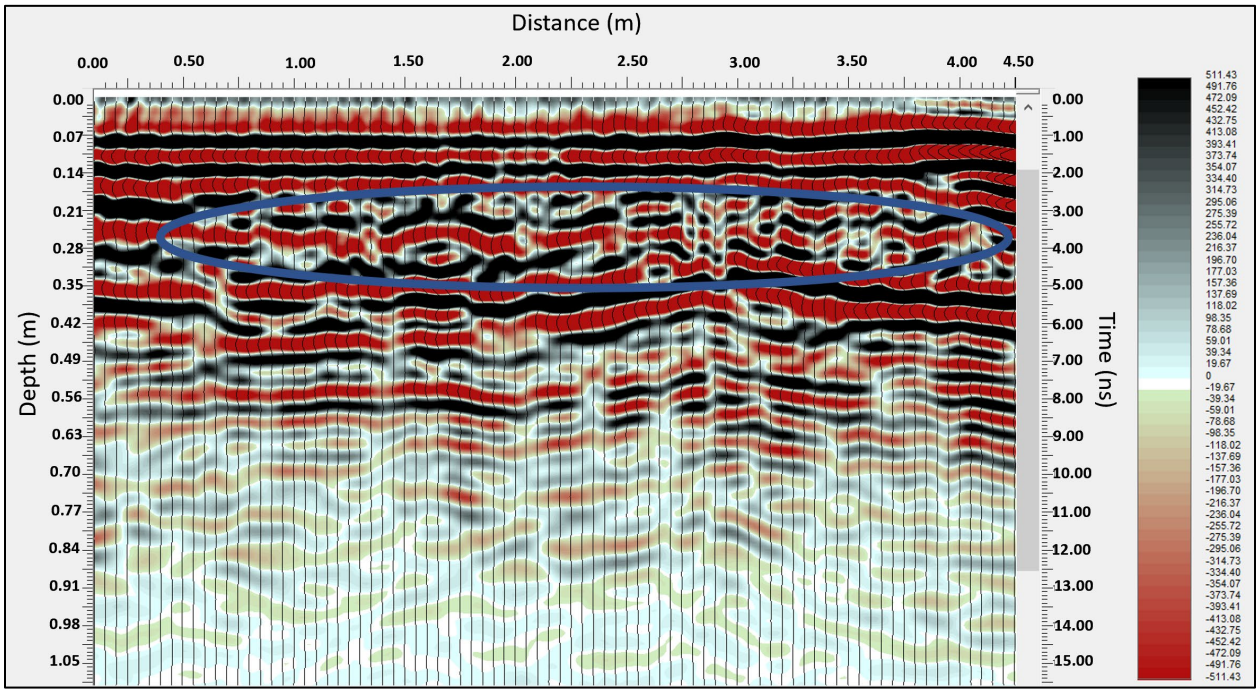

Figure 5. 2: 1 GHz frequency GPR 2D slices circle the location of the third (A) and fourth (B) distinctive characteristics identified across the survey area. (A) represents ichnofossils or sheetwash and (B) represents possible large ichnofossils or laterally extensive sheetwash.

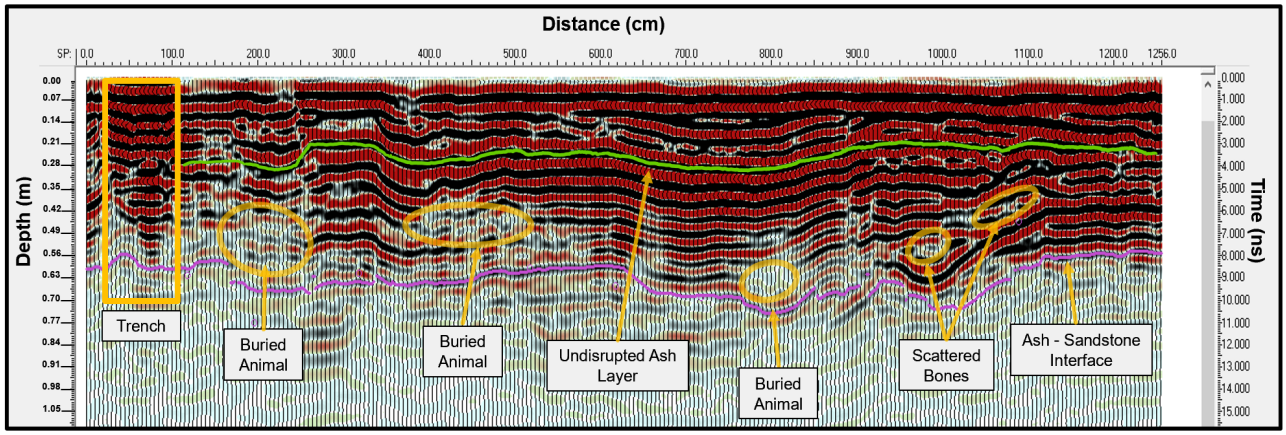

Figure 5. 3: GPR profile from quadrant Q with annotations of interpretated anomalies. Each of the markers identified as buried animals is compatible to characteristic 1. The green horizon is interpreted as a continuous ash layer within the Dead Zone. The purple horizon is the ash-sandstone contact.

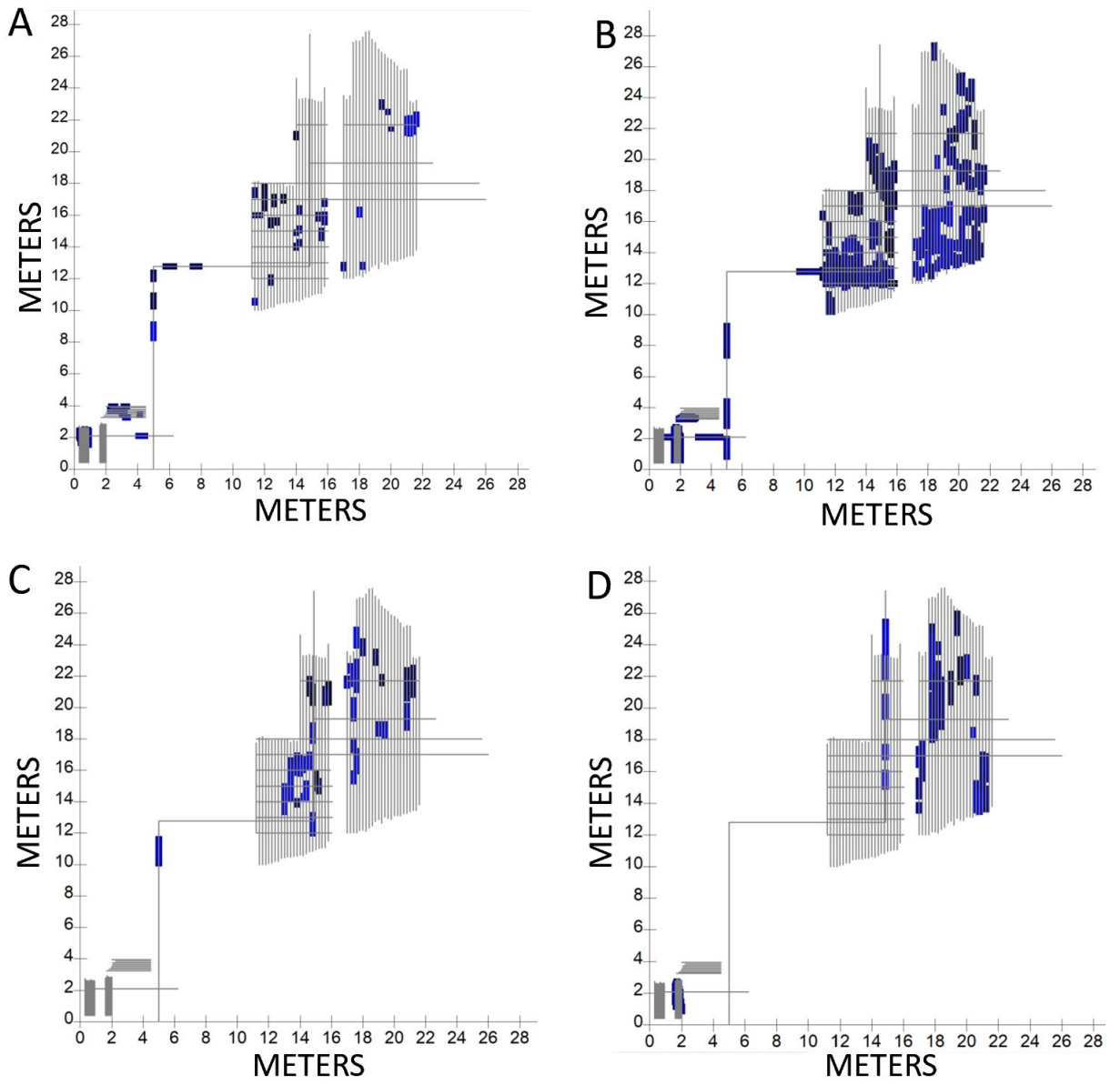

Figure 5. 4 (A-D): Maps showing the locations of the four GPR reflector signatures (highlighted in blue) within the ash beds. The first signature (A), second signature (B), third signature (C) and fourth signature (D) correspond to GPR reflector signals shown in Figures 5.1 and 5.2.

Chapter 6. Conclusions

Overall, GPR was successful at identifying the ash-sandstone contact, the locations of buried fossilized animal remains, and the possible locations of ichnofossils across the Ashfall Fossil Beds site. The results presented in Chapter 2 revealed that buried fossilized animal remains are associated with loss of amplitude and discontinuous reflections within the volcanic ash, which presents as continuous, strong amplitude reflections. In Chapter 3, I determined that GPR was able to successfully map the depth to the Cap Rock Member sandstone within the Hubbard Barn. The attenuation of the GPR amplitude strength corresponded to the ash-sandstone contact. In Chapter 4, the ability of the GPR to detect ichnofossils, such as animal burrows, within the shallower units of the volcanic ash deposits was tested. The GPR was able to detect the edges of a known animal burrow, represented by a discontinuity in the reflectors along the edges of the burrow. Future excavation of the animal burrow will allow for additional ground-truthing of these results and provide insight on the depths and orientation of this subvertical burrow. Lastly, in Chapter 5, the results of the first three chapters were combined to identify four GPR characteristics. The first two characteristics are related to the animal skeletal remains located within the Skeleton Zone across the site. The last two characteristics are related to the ichnofossils that are located within the Dead Zone across the site. By plotting out the locations of these individual characteristics, paleontologists can target future excavations to locate different types of fossils at the Ashfall Fossil Bed site.

Overall, the 1 GHz GPR frequency data offer the best resolution for identifying animal skeletons and ichnofauna in the subsurface ash. However, the 1 GHz antenna lost amplitude strength at a shallower depth, which made interpretation of the ash-sandstone contact more difficult than the 500 MHz data. The 500 MHz data provided more accurate interpretations of the

depth to the ash-sandstone contact. Also, the 500 MHz data could be used to identify areas of interpreted animal skeletal remains, but it was more difficult to interpret ichnofossils with this lower frequency. For future GPR surveys, I recommend deploying both the 500 MHz and 1 GHz frequency antennas to detect more fossilized skeletal remains, and the 1 GHz frequency antennas should be used to locate ichnofossils. Both frequencies are effective at identifying the transition from ash deposits to the underlying sandstone.

To validate the results of my study, future excavations at the Ashfall Fossil Beds site should be compared to the results of the GPR datasets for additional ground-truthing. Also, fossilized animal bones should be collected and analyzed to determine their dielectric and electrical properties, porosity, and mineral composition. Knowing more about the physical and chemical properties of the bones would facilitate our understanding of the detection capabilities of GPR to detect fossilized remains. Additionally, more research is needed to understand what affects the rates of fossilization, including the type of rock that encases the fossils. Ashfall is unique because the fossilized remains are contained in a high silica content volcanic ash, which works well with the GPR. Other environments, such as limestone or sandstone, may not be as compatible with GPR for detecting fossilized remains and should be further explored.

References

Aziz, A.S., Stewart, R. R., Green, S. L, and J. B. Flores, 2016, Locating and characterizing burials using 3d ground-penetrating radar (gpr) and terrestrial laser scanning (tls) at the Historic Mueschke Cemetery, Houston, Texas: Journal of Archaeological Science: Reports, **8**, 392–405, accessed August 5, 2021; https://doi.org/10.1016/j.jasrep.2016.06.035.

Annan, A.P., 2003, Ground penetrating radar: principles, procedures, & applications: Sensors &Software Inc. Technical Paper.

Balanis, C. A., 2012, Advanced engineering electromagnetics: Wiley.

Barone, P. M., Bellomo, T., Mattei, E., Lauro, S. E., and E. Pettinelli, 2011, Ground-penetrating radar in the regio III (Pompeii, Italy): archaeological evidence: Archaeological Prospection, **18**, 187–194, accessed August 5, 2021; https://doi.org/https://doi.org/10.1002/arp.405.

Cagnoli, B., and J. K. Russell, 2000, Imaging the subsurface stratigraphy in the Ubehebe hydrovolcanic field (Death Valley, California) using ground penetrating radar: Journal of Volcanology and Geothermal Research, **96**, 45–56, accessed August 5, 2021; https://doi.org/10.1016/s0377-0273(99)00142-0.

Damiata, B. N., Steinberg, J. M., Bolender, D. J., and G. Zoëga, 2013, Imaging skeletal remains with ground-penetrating radar: comparative results over two graves from Viking Age and Medieval churchyards on the Stóra-Seyla Farm, northern Iceland: Journal of Archaeological Science, **40**, 268–278, accessed August 5, 2021; https://doi.org/10.1016/j.jas.2012.06.031.

Davis, J. L., and A. P. Annan, 1989, Ground-penetrating radar for high-resolution mapping of soil and rock stratigraphy: Geophysical Prospecting, **37**, 531–551, accessed August 5, 2021; https://doi.org/10.1111/j.1365-2478.1989.tb02221.x.

Gillette, D., 1994, Seismosaurus: the earth shaker: Columbia University Press.

Gómez-Ortiz, D., Martín-Velázquez, S., Martín-Crespo, T., Márquez, A., Lillo, J., López, I., and F. Carreño, 2006, Characterization of volcanic materials using ground penetrating radar: a case study at Teide Volcano (Canary Islands, Spain): Journal of Applied Geophysics, **59**, 63–78, accessed August 5, 2021; https://doi.org/10.1016/j.jappgeo.2005.07.007.

Grandjean, G., de Marliave, C., Buigues, B., Mol, D., and G. Ruffie, 2002, Searching out mammoth remains in permafrost (Taimyr, Siberia) using ground penetrating radar: Ninth International Conference on Ground Penetrating Radar, **4758**, 675–678, accessed August 5, 2021; https://doi.org/10.1117/12.462270.

Hansen, J. D., Pringle, J.K., and J. Goodwin, 2014, GPR and bulk ground resistivity surveys in graveyards: locating unmarked burials in contrasting soil types: Forensic Science International, **237**, 14-29, accessed August 5, 2021; https://doi.org/10.1016/j.forsciint.2014.01.009.

Jol, H. M., 2009, Ground penetrating radar theory and applications: Elsevier.

Keenan, S.W., 2016, From bone to fossil: a review of the diagenesis of bioapatite: American Mineralogist, **101**, 1943-1951, accessed August 5, 2021; https://doi.org/10.2138/am-2016-5737

Leucci, G., De Giorgi, L., Di Giacomo, G., Ditaranto, I., Miccoli, I., and G. Scardozzi, 2016, 3D gpr survey for the archaeological characterization of the ancient Messapian necropolis in Lecce, South Italy: Journal of Archaeological Science: Reports, **7**, 290–302, accessed August 5, 2021; https://doi.org/10.1016/j.jasrep.2016.05.027.

Lukjanov, S.P., Stepanov, R.A., Chernyi, I.A., and O.V. Stukach, 2007, Use of the ground penetrating radar methods for paleontology on example of the mammoth fauna investigation: Proceedings of the 37th European Microwave Conference, 1747-1750.

Lyman, R. L., 1994, Vertebrate taphonomy: Cambridge University Press.

Main, D. J., and W. S. Hammon, 2003, The application of ground penetrating radar as a mapping technique at vertebrate fossil excavations in the Cretaceous of Texas: Cretaceous Research, **24**, 335–345, accessed August 5, 2021; https://doi.org/10.1016/s0195-6671(03)00047-8.

Makino, K.I., and H. Miura, 2005, Location of mammoth remains in perma-frost of northern Siberia using gpr and multifrequency em: Symposium on the Application of Geophysics to Engineering and Environmental Problems, 466-472.

Oguchi, T., Udagawa, M., Nanba, N., Maki, M., and Y. Ishimine, 2009, Measurements of dielectric constant of volcanic ash erupted from five volcanoes in Japan: IEEE Transactions on Geoscience and Remote Sensing, **47**, 1089–1096, accessed August 5, 2021; https://doi.org/10.1109/tgrs.2008.2008023.

Pettinelli, E., Barone, P. M., Di Matteo, A., Mattei, E., and S. E. Lauro, 2012, Mapping the undiscovered ruins of Pompeii (Naples, Italy) using ground penetrating radar:

Archaeometry, **54**, 203–212, accessed August 5, 2021; https://doi.org/10.1111/j.1475-4754.2011.00599.x.

Pringle, J. K., Ruffell, A., Jervis, J. R., Donnelly, L., Mckinley, J., Hansen, J., Morgan, R., Pirrie, D., and M. Harrison, 2012, The use of geoscience methods for terrestrial forensic searches: Earth-Science Reviews, **114**, 108–123, accessed August 5, 2021; https://doi.org/10.1016/j.earscirev.2012.05.006.

Russell, J. K., and M. V. Stasiuk, 1997, Characterization of volcanic deposits with ground-penetrating radar: Bulletin of Volcanology, **58**, 515–527, accessed August 5, 2021; https://doi.org/10.1007/s004450050159.

Schneider, B.B., and G. P. Tsoflias, 2017, GPR polarization effects of buried bison bone: SEG Technical Program, Expanded Abstracts, 5135-5139.

Schneider, B. B., 2017, GPR imaging of prehistoric animal bone-beds: PhD. Dissertation, University of Kansas.

Schultz, J. J., and T. L. Dupras, 2008, The contribution of forensic archaeology to homicide investigations: Homicide Studies, **12**, 399–413, accessed August 5, 2021; https://doi.org/10.1177/1088767908324430.

Seilacher, A., 1970, Begriff und bedeutung der fossil-lagerstätten: neues jahrbuch fur geologie und paläontologie: Monatshefte.

Skinner, M. F., Johnson, F.W., and C. Frick, 1984, Tertiary stratigraphy and the Frick collection of fossil vertebrates from north-central Nebraska: American Museum of Natural History Bulletin, **178**, 217-368, accessed August 5, 2021; http://hdl.handle.net/2246/332.

Skinner, M.F., Skinner S.M., Gooris R.J., 1968, Cenozoic rocks and faunas of Turtle Butte, south-central South Dakota: Bulletin of the American Museum of Natural History, **138**, 381–436, accessed August 5, 2021; http://hdl.handle.net/2246/1110.

Smith, J. J., Turner, E., Möller, A., Joeckel, R. M., and R. E. Otto, 2018a, First U-Pb zircon ages for Late Miocene ashfall Konservat-Lagerstätte and Grove Lake ashes from eastern Great Plains, USA: Plos One, **13,** accessed August 5, 2021; https://doi.org/10.1371/journal.pone.0207103.

Smith, J. J., Joeckel, R.M., Otto, R.E., and S.T. Tucker, 2018b, Life in the dead zone: A diverse Miocene ichnofauna preserved in volcanic ash, ashfall fossil beds state historical park, Nebraska: USA Geological Society of America, Abstracts with Programs.

Tinelli, C., Ribolini, A., Bianucci, G., Bini, M., and W. Landini, 2012, Ground penetrating radar and palaeontology: the detection of sirenian fossil bones under a sunflower field in Tuscany (Italy): Comptes Rendus Palevol, **11**, 445–454, accessed August 5, 2021; https://doi.org/10.1016/j.crpv.2012.04.002.

Tzanis, A., 2016, MatGPR R3.1, Computer software. MATGPR R-3.5; http://users.uoa.gr/~atzanis/matgpr/matgpr.html.

Tucker, S.T., Otto, R.E., Joeckel, R.M., and M.R. Voorhies, 2014, The geology and paleontology of Ashfall Fossil Beds, a Late Miocene (Clarendonian) mass-death assemblage, Antelope County and adjacent Knox County, Nebraska, USA: Geological Society of America, **36**, accessed August 5, 2021; https://doi.org/10.1130/2014.0036(01).

Udphuay, S., Thapchim, J., Ditbanjong, P., Yawichai, A., and P. Chanthasit, 2020, Ground-penetrating radar for fossil investigation, Phu Noi excavation site, Thailand: 18th International Conference on Ground Penetrating Radar, 287-290.

Urban, T. M., Bennett, M.R., Bustos, D., Manning, S.W., Reynolds, S.C. Matteo Belvedere, M., Odess, D., and V. L. Santucci, 2019, 3-D radar imaging unlocks the untapped behavioral and biomechanical archive of Pleistocene ghost tracks: Scientific Reports, **9**, accessed August 5, 2021; https://doi.org/10.1038/s41598-019-52996-8.0.

Voorhies, Mike R., 1985, A Miocene rhinoceros' herd buried in volcanic ash: National Geographic Society Research Reports, **19**, 671–688, accessed August 5, 2021; https://www.rhinoresourcecenter.com/pdf_files/137/1378684580.pdf.

Voorhies, M., Otto, R., Mosel, S., and S. Tucker, 2016, Ashfall Fossil Beds State Historical Park and national natural landmark: present view of an ancient past: The Board of Regents of The University of Nebraska.

Zhao, W., Forte, E., Fontana, F., Pipan, M., and G. Tian, 2018, GPR imaging and characterization of ancient roman ruins in the Aquileia Archaeological Park, NE Italy: Measurement, **113**, 161–171, accessed August 5, 2021; https://doi.org/10.1016/j.measurement.2017.09.004.

Appendix

TABLE 1. HISTORY OF ASHFALL FOSSIL BEDS AND PALEONTOLOGICAL EXPLORATION OF ENCLOSING AREA

1796	James MacKay finds first fossil from Niobrara River valley (Nasatir, 1952; Diller, 1955)
1857	Ferdinand V. Hayden collects specimens from Niobrara River valley
1858	Joseph Leidy describes first fossils from Niobrara River valley
1926–1980	Morris Skinner develops biostratigraphic framework of the Niobrara valley
1953	UNSM field party collects articulated *Teleoceras major* skull and jaws from the Ashfall hillside
1971	Michael Voorhies discovers first intact *Teleoceras major* skeleton from volcanic ash
1977	UNSM field crew uncovers 11 more articulated *Teleoceras major* skeletons from ash
1978–1979	National Geographic Society funds further excavations in ash; 120 skeletons of multiple vertebrate taxa recovered
1991	Ashfall Fossil Beds State Park opens to the public
2006	U.S. Department of Interior designates Ashfall a National Natural Landmark
2009	Hubbard Family Rhino Barn opens; excavations continue to present day

UNSM—University of Nebraska State Museum.

Table A1: History of Ashfall Fossil Beds site and paleontological exploration of the area (Tucker et al., 2014).

TABLE 2. PALEOFLORA AND FAUNA LIST FROM LAGERSTÄTTE-BEARING ASH AND THE UNDERLYING SAND AT ASHFALL FOSSIL BEDS

Taxa	Common name	In ash bed	Ingested	Sand below
Plants				
Equisetum sp.	Horsetail rush	-	-	X
Carex graceii	Sedge	-	-	X
Cyperocarpus pulcherrima	Sedge	-	-	X
Cyperocarpus terrestris	Sedge	-	-	X
Berriochloa communis	Grass	-	X	X
Berriochloa primaeva	Grass	-	X	-
Paleoeriocoma hitchcockii	Grass	-	-	X
Juglandicarya sp.	Walnut	-	-	X
Celtis occidentalis	Hackberry	-	-	X
Cryptantha auriculata	Borage	-	-	X
Fish				
Osteichthyes (Gen. et sp. indet.)	Minnow-sized bony fish	-	-	X
Amphibians				
Ambystoma minshalli	Extinct salamander	-	-	X
Ambystoma tigrinum	Tiger salamander	-	-	X
Bufo valentinensis	Extinct toad	-	-	X
cf. *Lithobates pipiens*	Leopard frog	-	-	X
Reptiles				
Sternorthurus odoratus	Stinkpot turtle	-	-	X
Chrysemys n. sp.*	Painted turtle	SK	-	X
Hesperotestudo orthopygia	Giant tortoise	SK	-	X
Sceloporus sp. A	Fence lizard	-	X	-
Sceloporus sp. B	Fence lizard	-	X	-
Cnemidophorus cf. *C. sexlineatus*	Six-lined racerunner	-	X	X
Plestiodon sp.	Skink	-	X	X
Colubrid (Gen. et sp. indet.)	Common constrictor	SK	-	-
Paleoheterodon tiheni	Extinct hognose snake	-	-	X
Ameiseophis robinsoni	Extinct snake	-	-	X
Salvadora paleolineata	Extinct patch-nose snake	-	-	X
Nerodia sp.	Water snake	-	-	X
Thamnophis sp.	Garter snake	-	-	X
Viperid (Gen. et sp. indet.)	Pit viper	-	-	X
Birds				
*Balearica exigua**	Extinct crowned crane	SK	-	X
*Apatosagittarius terrenus**	False secretary bird	X	-	X
*Anchigyps voorhiesi**	Old World vulture	X	-	-
Rallid (Gen. et sp. indet.)	Rail	X	-	X
Passerine (Gen. et sp. indet.)	Small songbird	-	-	X
Mammals				
Ochotonidae				
Gen. et sp. indet.	Pika	-	-	X
Leporidae				
Hypolagus cf. *H. fontinalis*	Small rabbit	-	-	X
Hypolagus sp.	Large rabbit	-	-	X
Mylagaulidae				
Ceratogaulus cf. *C. anecdotus*	Horned rodent	B	-	X
Sciuridae				
Spermophilus (*Otospermophilus*) *cyanocittus*	Small ground squirrel	B	-	X
Ammospermophilus junturensis	Large ground squirrel	-	-	X
Castoridae				
Eucastor sp.	Round-tailed beaver	-	-	X
Cricetidae				
Copemys sp.	Deer mouse	-	X	X
Sigmodontine (N. Gen. et sp.)*	Large mouse	-	-	X
Geomyoidea				
Phelosaccomys hibbardi	Gopher	-	-	X
Heteromyidae				
Cupidinimus sp.	Pocket mouse	-	-	X
Mioheteromys cf. *M. amplissimus*	Large pocket mouse	-	-	X
Perognathus cf. *P. minutus*	Small pocket mouse	-	-	X
Canidae				
Aelurodon sp.	Wolf-sized bone-crushing dog	-	-	X
Carpocyon cf. *C. webbi*	Fruit-eating dog	-	-	X
Epicyon cf. *E. haydeni*	Large bone-crushing dog	-	-	X
Epicyon cf. *E. saevus*	Small bone-crushing dog	-	-	X
Cynarctus cf. *C. voorhiesi*	"Raccoon" dog	SK	-	X
Leptocyon sp.	Fox-sized dog	X	-	X
Amphicyonidae				
Ischyrocyon cf. *I. gidleyi*	Beardog	-	-	X

TABLE 2. PALEOFLORA AND FAUNA LIST FROM LAGERSTÄTTE-BEARING ASH AND THE UNDERLYING SAND AT ASHFALL FOSSIL BEDS (*Continued*)

Taxa	Common name	In ash bed	Ingested	Sand below
Mustelidae				
Leptarctus sp.	Koala-like carnivore	-	-	X
Erinaceidae				
Untermannerix copiosus	Moonrat	-	-	X
Metechinus nevadensis	Large hedgehog	-	-	X
Talpidae				
Domninoides n. sp.*	Giant mole	-	-	X
Gen. et sp. indet.	Small mole	X	-	X
Soricidae				
Gen. et sp. indet.	Shrew	-	-	X
Vespertilionidae				
Myotis sp.	Bat	-	-	X
Tayassuidae				
"*Prosthennops*" sp.	Peccary	-	-	X
Merycoidodontidae				
Ustatochoerus skinneri	Oreodont	-	-	X
Camelidae				
Protolabis heterodontus	Llama-like camel	SK	-	X
Procamelus grandis	Ancestral camel	SK	-	X
Megatylopus sp.	Large camel	X	-	X
Aepycamelus sp.	Giraffe-like camel	X	-	X
Gelocidae				
Pseudoceras sp.	Small hornless ruminant	-	-	X
Moschidae				
Longirostromeryx wellsi	Musk deer	SK	-	X
Antilocapridae				
cf. *Proantilocapra* sp.	Pronghorn antelope	-	-	X
Palaeomerycidae				
Cranioceras sp.	Three-horned "deer"	-	-	X
Equidae				
Pseudhipparion gratum	Small three-toed horse	SK	-	X
Neohipparion affine	Slender three-toed horse	SK	-	X
Cormohipparion occidentale	Stout three-toed horse	SK	-	X
? *Protohippus simus*	Slender one-toed horse	SK	-	X
Pliohippus pernix	Stout one-toed horse	SK	-	X
Rhinocerotidae				
Aphelops sp.	Hornless rhinoceros	-	-	X
Teleoceras major	Barrel-bodied rhinoceros	SK	-	X
Gomphotheriidae				
cf. *Eubelodon* sp.	Short-jawed four-tusker	-	-	X

Abbreviations: SK—intact skeletons; X—present; - —not present; B—present in burrow fills slightly post-dating airfall event.
*New species described from the site.
Paleobotanical data from Voorhies and Thomasson (1979) and Thomasson (1987); fish from Herbel (1994); amphibians from Holman (2000, personal commun.); reptiles from Holman (2000, personal commun.) and Head (2013, personal commun.); birds from Feduccia and Voorhies (1989, 1992) and Zhang et al. (2012); and mammals from Voorhies (1985, 1990b; personal observations), Herbel (1994), Korth (1997), Czaplewski et al. (1999), Mead (1999, 2000), and Wang et al. (1999).

Table A2: Table created by Tucker et. al [2014]. Appendix of the 21 different taxa found throughout the Ashfall site and recorded condition when located.

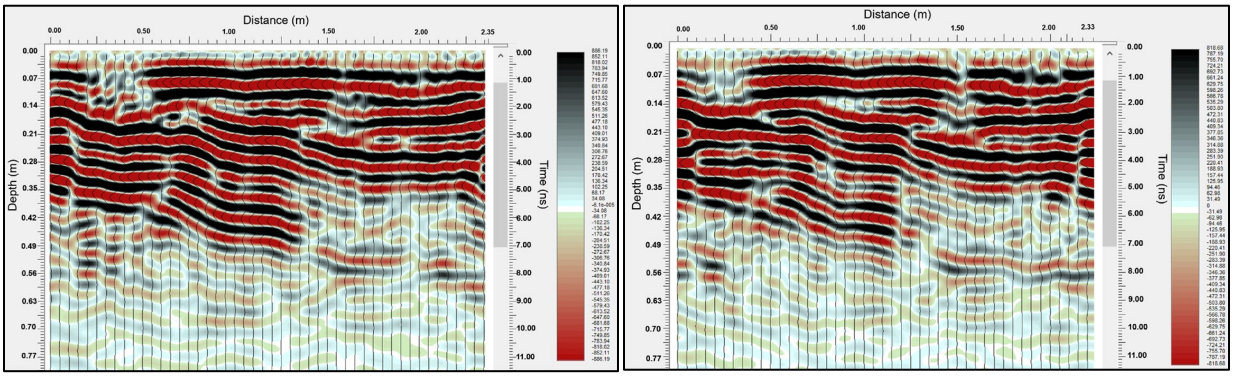

Figure A1: Line 00 (left) and 01 (right) are the first two lines of the GPR grid over the partially exposed jaw of the rhino collected by the 1 GHz frequency antennas. Amplitude strength of the GPR signal decreases abruptly at the sandstone-ash contact around 50-60 cm below the surface.

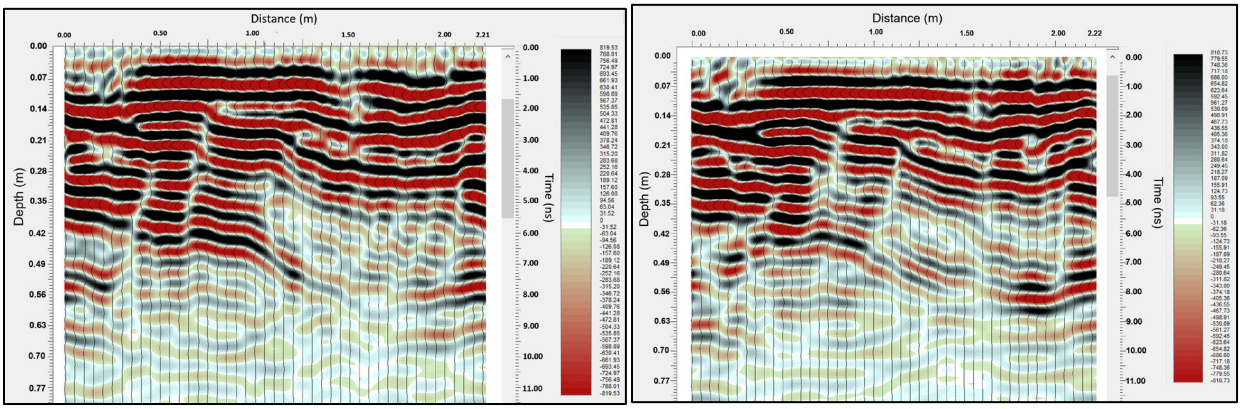

Figure A2: Lines 03 (left) and 04 (right) are from the middle area of the GPR grid, which includes the estimated location of the lower jaw and neck of the buried rhino.

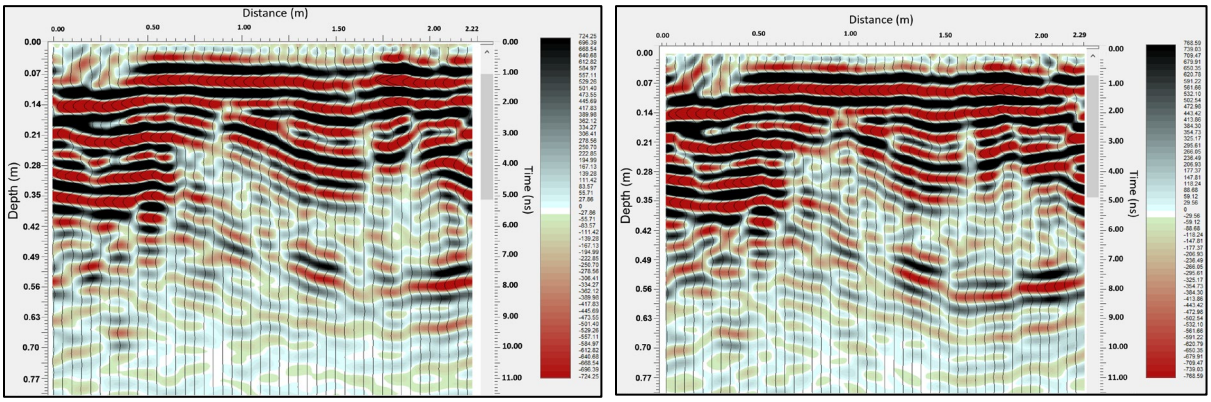

Figure A3: Lines 06 (left) and 07 (right) are from the middle area of the GPR grid, which includes the estimated location of the neck and shoulder of the buried rhino.

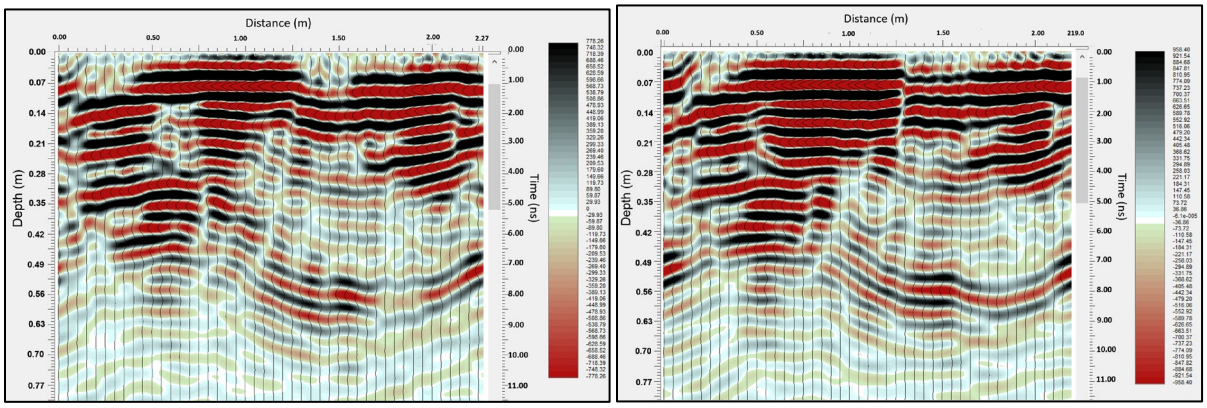

Figure A4: Lines 11 (left) and 12 (right) are over the estimated location of the rhinoceros's ribcage.

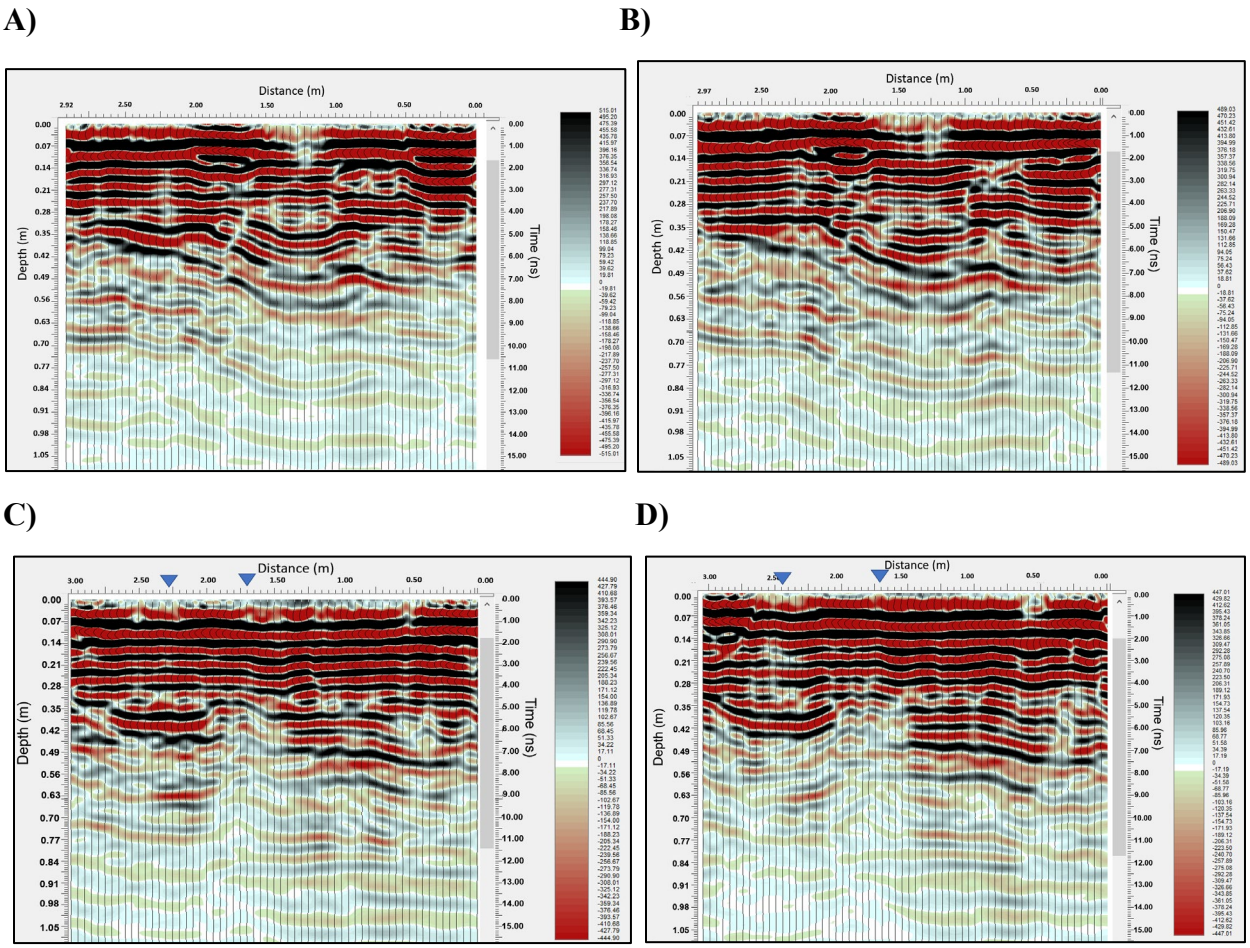

Figure A5: (A) Line 1 (A) and line 2 (B) are 1 GHz frequency GPR profiles over the surface expression of the animal burrow. Line 3 (C) and line 4 (D) intersect the burrow on the surface at the locations marked by the blue triangles. The orange arrow identifies disruptions beneath intersecting animal burrow. The yellow boxes represent low amplitude and discontinuous reflectors below the blue triangles.

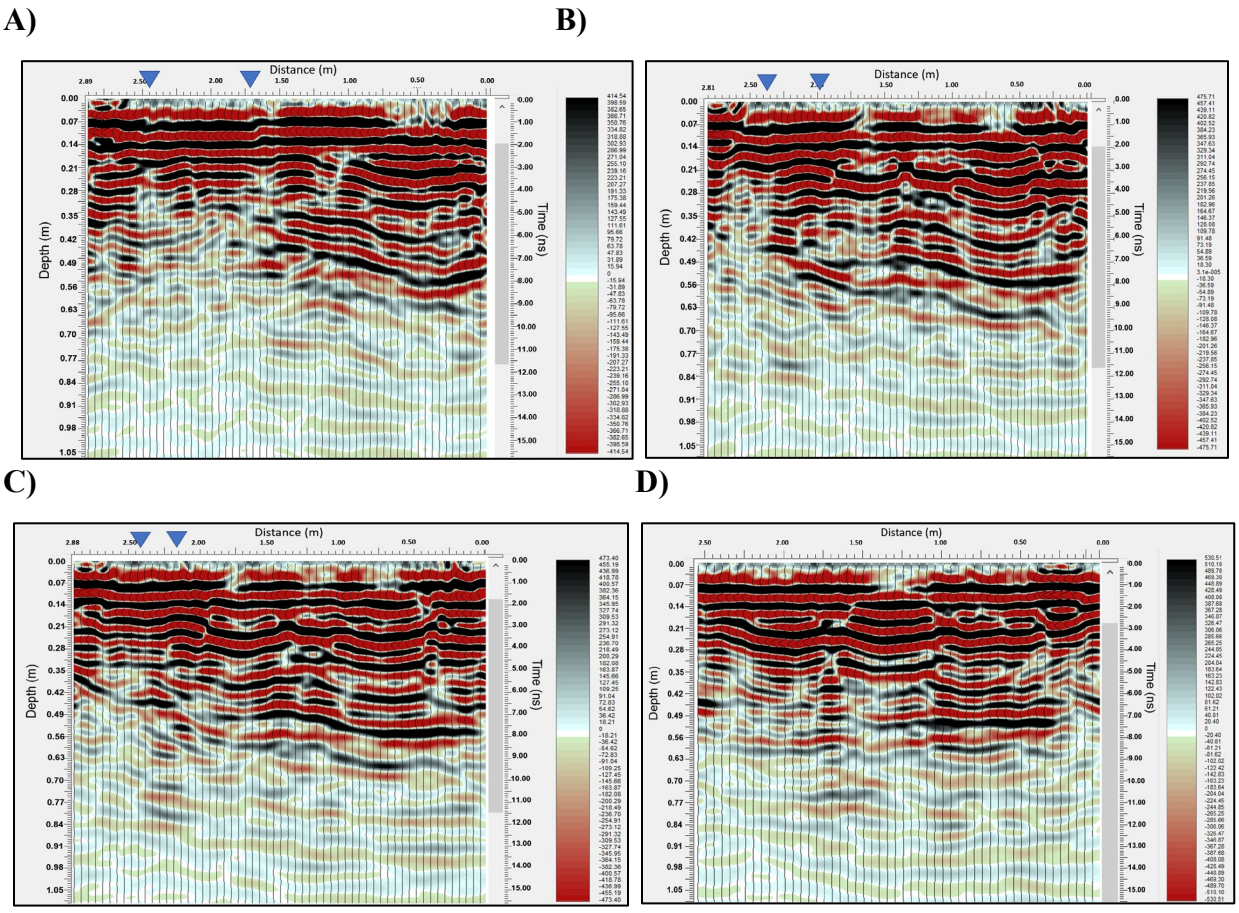

Figure A6: Annotated 1 GHz frequency GPR lines 5-8 (A-C) indicating the location a burrow between the blue triangles. Line 8 (D) does not intersect the burrow on the surface by the GPR. The orange arrow identifies disruptions beneath intersecting animal burrow. The yellow boxes represent low amplitude and discontinuous reflectors below the blue triangles.

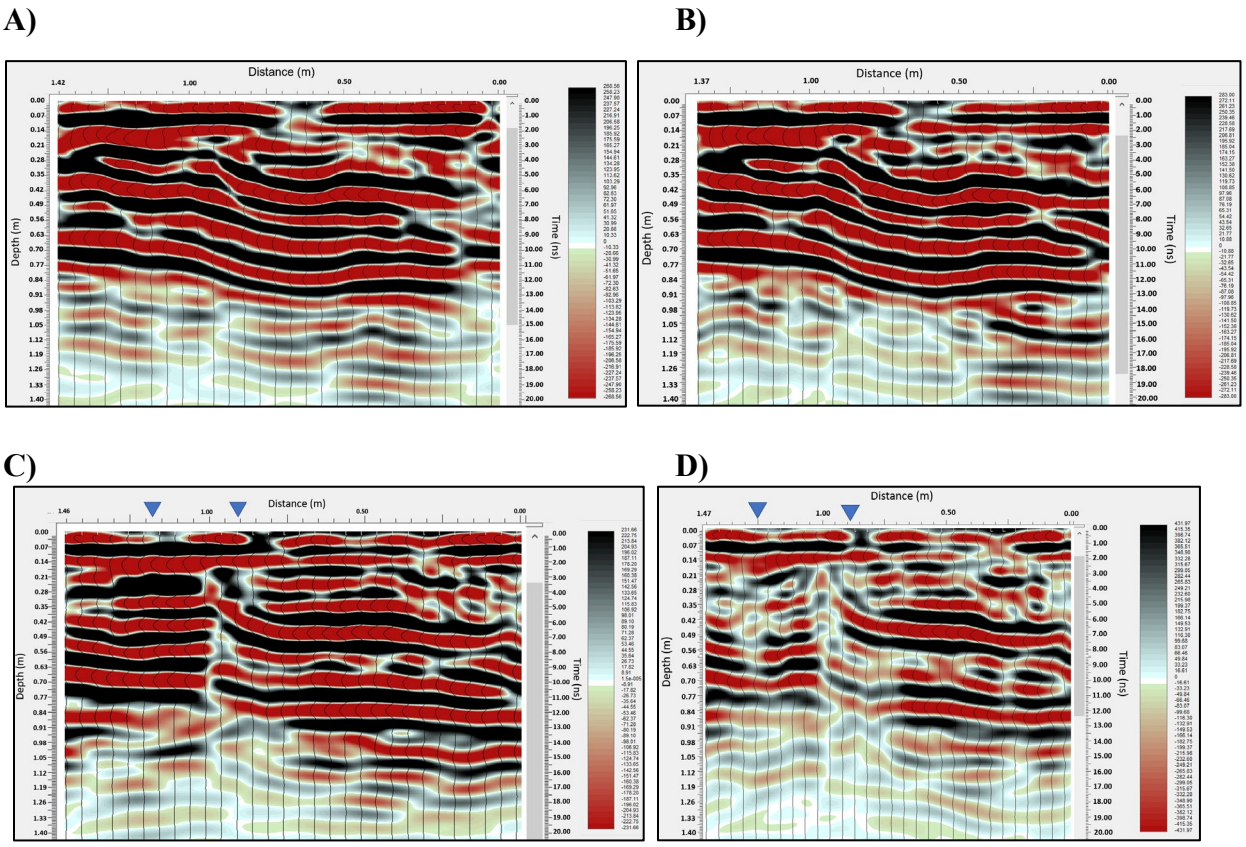

Figure A7: Line 1 (A) and line 2 (B) are 500 MHz frequency GPR profiles over the surface expression of the animal burrow. Line 3 (C) and line 4 (D) intersect the burrow at the locations marked by the blue triangles. The orange arrow identifies disruptions beneath intersecting animal burrow. The yellow boxes represent low amplitude and discontinuous reflectors below the blue triangles.

A) B)

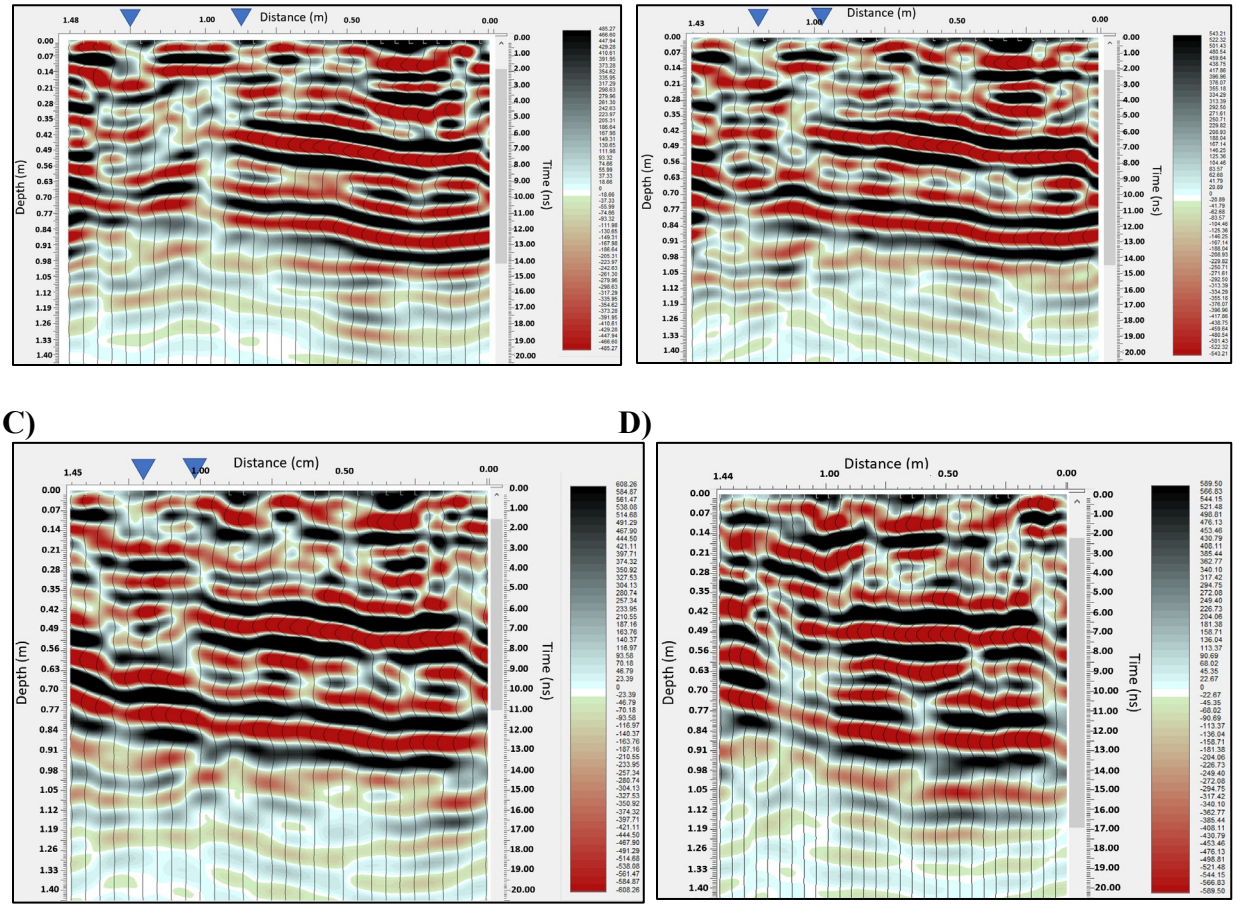

C) D)

Figure A8: Annotated 500 MHz frequency GPR lines 5-8 (A-C) indicating the location a burrow between the blue triangles and circled area is the suspected profile of the animal burrow. Line 8 (D) does not cross over the burrow. The orange arrow identifies disruptions beneath intersecting animal burrow. The yellow boxes represent low amplitude and discontinuous reflectors below the blue triangles.